Frustrated and Realized Hydrogen Bonding in 4-Hydroxy-3,5-di*tert*butylphenylphosphine Derivatives

Flávia Marszaukowski,[1,2] René T. Boeré*[2] and Karen Wohnrath*[1]

[1] Departamento de Química, Universidade Estadual de Ponta Grossa, Av. Gal. Carlos Cavalcanti, 4748, Uvaranas, CEP, 84030-900, Ponta Grossa, PR, Brazil.

[2] Department of Chemistry and Biochemistry and the Canadian Centre for Research in Advanced Fluorine Technologies, University of Lethbridge, 4401 University Dr. W, Lethbridge, AB, Canada T1K 3M4

Corresponding authors: Prof. René T. Boeré (email: boere@uleth.ca)
Prof. Karen Wohnrath (email: karen.woh@gmail.com)

Journal: Crystal Growth & Design

Manuscript ID: cg-2022-00020w

Abstract

Synthesis, molecular and supramolecular structures of a series of triarylphosphines $P(Ph)_{3-n}\{4\text{-}RO\text{-}3,5\text{-}(^tBu)_2\text{-}C_6H_2\}_n$ (*n* = 1, 3; R = $SiMe_3$, H) are reported. Chemical oxidation products $E{=}P(Ph)_{3-n}\{4\text{-}RO\text{-}3,5\text{-}(^tBu)_2\text{-}C_6H_2\}_n$ (E = O, S and Se; *n* = 1, 3; R = $SiMe_3$, H) are also reported. Crystal structures of the reported compounds were determined by single-crystal X-ray diffraction, using a Hirshfeld Atom Refinement with NoSpherA2 through OLEX2, which provides an average improvement in C–C bond distance precision of 35%. Phosphine basicity for the phosphines with *n* = 1, R = H and *n* = 3, R = $SiMe_3$, H was determined using the $^1J_{P,Se}$ values of the respective selenides; $^1J_{P,Se}$ = 699 Hz for E = Se; *n* = 3; X = H identifies the most basic triarylphosphine ever reported. Intermolecular interactions allow classification of the 17 structures into 4 categories: those with only dispersion-induced short contacts; those with frustration of H-bonding; those with only classic H-bonding and those with combinations of classic and frustration of H-bonding. A "double phenol embrace" classified by an $R_2^2(4)$ graph set is a weak intermolecular synthon organizing lattices with 2,6-di*tert*butylphenol functional groups. Classic H-bonding occurs only when E = O.

Introduction

Organophosphines are amongst the most versatile and broadly applied ligands in transition metal coordination chemistry, reacting with a wide variety of metals over a range of oxidation states.[1-4] Triarylphosphines including PPh_3 itself are the most commonly used phosphine ligands largely due to ease of handling and low costs of production. Consequently, variation in secondary functional groups on aryl rings in Ar_3P now cover a vast range of substituent types including those with electronic influence on the phosphine donor strength (electron donating versus withdrawing) or solubility modifiers (lipophilic or hydrophilic modifiers).[5] An important theme over the past decades has been on triarylphosphines with substituents that can support even aqueous solubility of neutral metal complexes of such phosphines, and facilitating catalysis in water.[6] Phenolic phosphines such as $Ph_2PC_6H_4OH$ have been used either natively or with chain extenders such as triethylene glycol to enhance solubility for a ruthenium complex for catalysis in water.[7] The confinement of triarylphosphines in microenvironments leading to enhanced performance of catalytic processes,[8] as well as a number of studies aimed at enhanced anticancer activity also of ruthenium complexes,[9-13] have been reported.

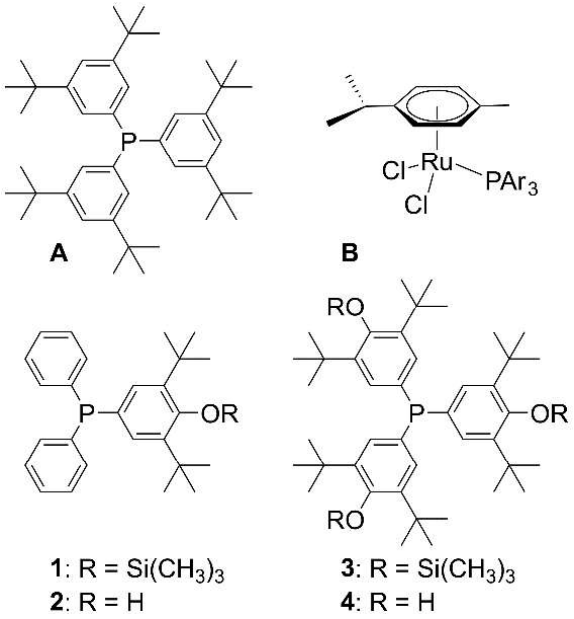

Chart 1

Recently, the highly lipophilic triarylphosphine **A** (Chart 1),[14] when employed in an [(η^6-cymene)RuX_2PAr_3] complex of type **B**, was shown to have promising behavior for cytotoxic activity in human cancer cell lines (MDA-MB-231 and A549) and little effect against the non-tumor cells line MRC-5, which is an indication of possible selective attack on cancerous cells.[15] Encouraged by these results, we decided to synthesize phosphines **2** and **4** (Chart 1), via precursors **1** and **3**, with the aim of using the

phenol functional groups in the subsequent complexes **B** as H-bond donors to water, and to create new sites of interaction with the biological environment, to enhance chemotherapeutic efficacy, while retaining the lipophilicity of the *tert*butyl groups in **A**. Phosphines **1**-**4** have been previously reported,[16,17] but in the intervening years no applications of them have been reported, and their crystal structures remain unknown. Here we report on the syntheses, molecular and supramolecular structures of **1** – **4**; we also pursued their chalcogenides (P=O, P=S and P=Se), since under biological conditions any phosphine ligands that might be displaced from their metals are expected to transform rapidly to the oxides; meanwhile, the selenides are useful to establish phosphine basicity via $^{1}J_{P,Se}$.

The molecular and crystal structures of all the compounds reported here (see Scheme 1) have been determined using single-crystal X-ray diffraction. Refinement of the crystallographic models was undertaken using non-spherical atomic scattering factors. The recently reported software package NoSpherA2,[18] which is fully incorporated into Olex2 release 1.5,[19] is claimed to be a robust approach to Hirshfeld Atom Refinement (HAR) with custom, aspherical atomic scattering factors. H-atom placement approximating to the precision of neutron diffraction is indicated, with significant improvements in the accurate placements of H atoms involved in hydrogen bonding and other kinds of intermolecular interactions, compared to conventional refinements using the independent atom model (IAM).[18] This paper was also conceived to test the accuracy and robustness claims of the new method on a set of otherwise 'ordinary' crystal data, albeit obtained from a state-of-the-art diffractometer with micro-focus X-ray sources (Cu and Mo) and a hybrid photon counting detector. Detailed reporting on the models developed with the help of NoSpherA2, the challenges encountered, and promising improvements in structure precision, is provided.

A noteworthy feature in many of these phenol-containing compounds are unusual intermolecular interactions that fail the generally accepted criteria for H-bonding.[20-22] Specifically, in all the structures of phosphine derivatives with three di*tert*butylphenol substituents, at least one and usually two of the phenolic OH groups fail to make *any* intermolecular contacts less than the sums of the respective van der Waals radii (hereafter: *short contacts*). Moreover, those short contact that do form are either symmetrical Ar-OH···OH-Ar contacts **C** (Chart 2) which fail classic H-bonding criteria because of severe steric shielding by the two neighboring *tert*butyl groups,[23] or are OH contacts to S=P or Se=P on a neighboring molecule. The type **C** contacts, which we have dubbed the "phenolic double embrace", constitute a possible supramolecular synthon for this compound class; an analysis of this interaction is presented.

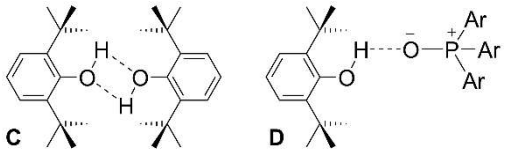

Chart 2

There is increasing interest in the literature in classifying and understanding circumstances in which functional groups *fully capable* of H-bonding fail to establish donor acceptor interactions. Collectively, such phenomena are being classified as the *frustration* of H-bonding.[24-29] Several scenarios have been outlined for this phenomenon. One is the case of a mismatch of the number of H-bond donors and acceptors,[24-26] another is when structural features prevent all the potential H-bonds from developing[27-28] and a third category is when functional groups normally capable of H-bonding do not do so, leading to the well-known PLATON Alert 'D-H without acceptor'.[29] In this study, the second and third occurrences of the frustration of H-bonding have been identified. By contrast, it was found that oxidation to phosphine oxides, whereby more accessible and stronger H-bond acceptors are formed (**D** in Chart 2), promotes the *realization* of conventional H-bonding, where structure **D** emphasizes the high polarity of phosphine oxides.

Results and discussion

Synthesis. All synthesized compounds (Scheme 1) were fully characterized by melting point and 1D and 2D NMR spectroscopy. ^{1}H, ^{31}P, ^{13}C, ^{1}H-^{1}H gCOSY, ^{1}H-^{13}C gHSQC and ^{1}H-^{13}C gHMBC NMR spectra are in full agreement with the structures shown (see the Experimental and the Supporting Information document, SI, for full details). Synthesis of the reagent 2,6-di*tert*butyl-4-bromophenoxy-trimethilsylane, used as a precursor in the synthesis of phosphines **1** and **3**, was recently optimized and its crystal structure reported.[30] The synthesis of **1** and **3** was enhanced from the original report by Pastor & Hessell [16] by employing the non-nucleophilic base ^{t}BuLi in place of ^{n}BuLi in the metal-halogen exchange reactions, significantly improving yields.

Phosphines **2** and **4** were obtained by the hydrolysis of **1** and **3**, respectively, through prolonged refluxing in a 10:1 mixture of methanol and water to ensure complete reactions. Phosphine **4** precipitated as a white solid with high purity upon cooling the synthesis mixture, while **2** required an additional washing and extraction step and, at the end of the work-up procedure, was also obtained with high purity. By contrast, Pastor & Hessell were not able to obtain **2** in a pure state and maintained that **4** required purification by preparative HPCL.[16]

Phosphine chalcogenides were obtained using standard methods.[31,32] The phosphine oxides **2c** and **4c** were synthesized by refluxing the phosphines with H_2O_2 in acetone. Phosphine sulfides **2a**, **3a** and **4a** and

selenides **2b**, **3b** and **4b** were obtained by heating the phosphines with the corresponding chalcogens in xylenes in order to overcome the low solubility of S and Se in organic solvents. We were unable to obtain oxides from phosphines with $OSi(CH_3)_3$ substituents (**1** and **3**) because under the oxidation conditions, hydrolysis of the siloxane functional groups occurred, resulting directly in **2c** and **4c** as products. In our hands, the sulfide and selenide of **1** could not be obtained as pure substances. Scheme 1 illustrates and summarizes all the synthetic transformations in this paper.

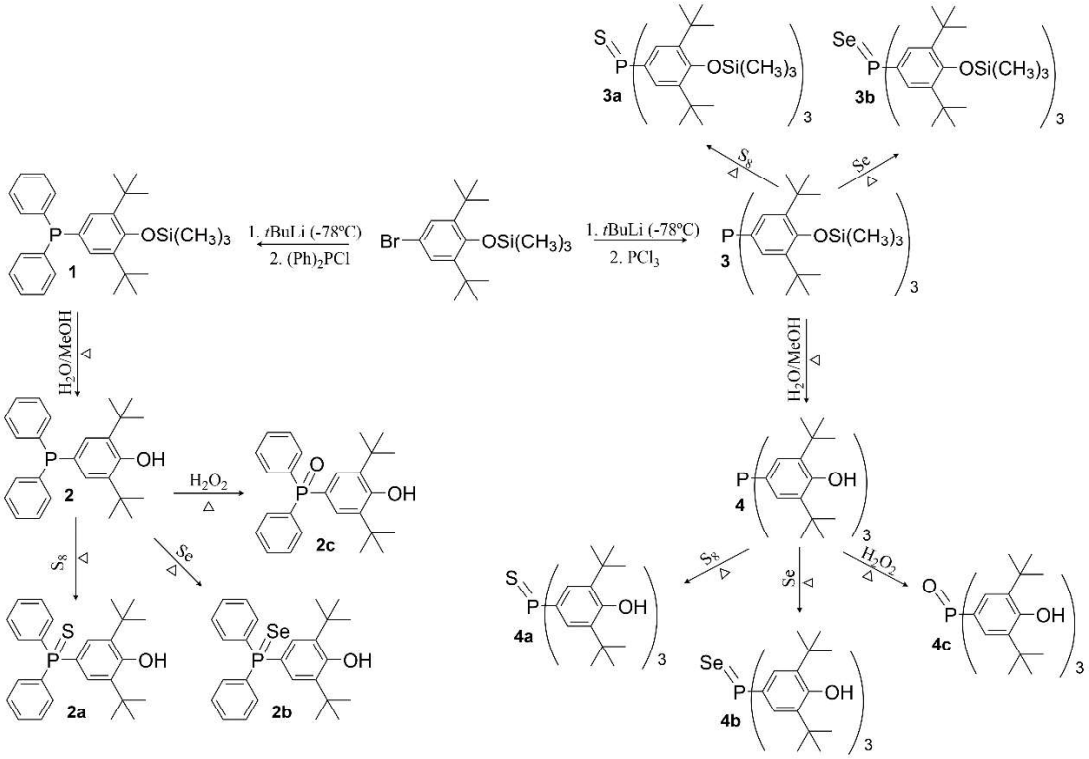

Scheme 1. Summary reaction scheme for the preparation of all the reported compounds

Table 1 presents the $^{31}P\{^1H\}$ NMR data. Higher frequency (shielding) is observed for the siloxanes **1** and **3** compared to phenols **2** and **4**; similarly, the *tris*-(3,5-di*tert*butylphenyl)-phosphines **3** and **4** are more shielded than the diphenyl phosphines **1** and **2**. Upon oxidation, the ^{31}P resonances are significantly shifted to lower frequencies. All the phosphine chalcogenide resonances show the expected relative $\delta\ ^{31}P\{^1H\}$: S > Se > O.[33] Considering the magnitudes of the changes in chemical shift ($\Delta\delta$) resulting upon oxidation, it is observed that all are consistently in the order, $\Delta\delta$ = **3** > **4** > **2**.

Table 1 $^{31}P\{^{1}H\}$ chemical shifts of synthesized phosphines (**1**-**4**) and their respective chalcogenides **a** – **c**.[a]

Phosphine	δ $^{31}P\{^{1}H\}$						
	P	P=S (**a**)	Δδ (ppm)	P=Se (**b**)	Δδ (ppm)	P=O (**c**)	Δδ (ppm)
1	-5.75	---	---	---	---	---	---
2	-4.88	43.75	+48.63	35.45	+40.33	31.01	+35.89
3	-9.15	42.89	+52.04	33.69	+42.89	---	---
4	-7.78	43.40	+51.18	34.61	+42.39	32.31	+40.09

[a] Δδ (ppm) = δ(P=E) – δ(P)

Phosphine basicity. The phosphine NMR data for **2b**, **3b** and **4b** also afford the opportunity to assess the basicity of their parent phosphines **2**, **3** and **4** using the $^{1}J_{P,Se}$ values of these selenides. This was previously done in the case of *tris*-(3,5-di*tert*butylphenyl)-phosphine (**A** in Chart 1).[14,34] Here we attempt to put these results into a broader context by comparing literature data on triarylphosphines for which $^{1}J_{P,Se}$ data are available (Table 2) with geometry-optimized and frequency-verified density functional theory (DFT) calculations at the B3LYP-D3BJ/6-31+G(2d,p) level of theory. Our prior work on **A** alerted us to the crucial importance of correcting for dispersion in such DFT calculations.[14,35] The analysis (Fig. 1) indicates a strong linear correlation between the computed HOMO (phosphorus lone pair) orbital energies and the $^{1}J_{P,Se}$ data of the corresponding phosphine selenides. We note, from a thorough search of the literature for comparative $^{1}J_{P,Se}$ data, that amongst this comparison series, **4** is the most basic triarylphosphine yet reported, with **3** as a close second. The fifth column of data in Table 2, the *deviation in sums of angles around P* is the amount, in °, that the $\sum\angle_{CPC}$ [35] is less than the average 304.1(5)° taken over all but **A**, **3** and **4**. These show a noticeable reduction in pyramidality attributed to dispersion (attraction between the *tert*butyl groups and aryl rings); note that the high basicity induced by the inductive effects of the substituents in these phosphines must overcome this reduction in the HOMO energy caused by rehybridization at P. Despite this handicap, **3** and **4** are very basic phosphines, comparable to mixed alkyl-aryl phosphines such as dicyclohexylphenylphosphine ($^{1}J_{P,Se}$ = 701.2 Hz for Cy_2PhP=Se, though the correlation between DFT-computed HOMO energies and $^{1}J_{P,Se}$ shown in Fig. 1 has as yet not been extended to mixed alkyl/aryl or all alkyl derivatives).[36] Table 2 also contains estimated pK_B values for all the phosphines, obtained from the $^{1}J_{P,Se}$ using the regression formula of Beckmann et al.[37] Hence by using straightforward computational chemistry, access can be obtained to good estimates for pK_B values.

Insert Table 2 near here.

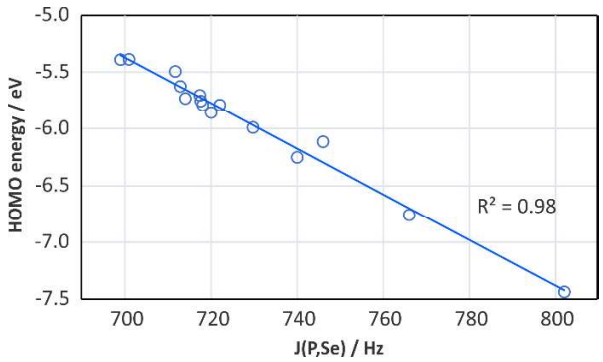

Figure 1. Correlation of the $^{1}J_{P,Se}$ coupling constants in Se=PAr_3 with the HOMO energy of the lowest conformation of the PAr_3 as computed at the B3LYP-D3BJ/6-31+G(2d,p) level of theory. Regression equation: $E_{HOMO} = -0.020 \times {}^{1}J_{P,Se} + 8.5$.

Crystal structures. A total of 17 crystal structures have been determined for this paper, including several variant structures of the same compound obtained from different crystallization conditions (for details, see Experimental and sections S1,5 in Supporting Information). Since these structures provide interesting variations in their supramolecular architectures, it was found significant to include all in the analysis. First, the unique features of each structure will be briefly described, grouped by compound type. Thereafter, a systematic analysis of the encountered supramolecular architectures will be provided.

In view of the vast amount of intramolecular distance and angle data and the significant parallelism of the obtained structures, it is not considered profitable to review such information structure by structure. Fortunately, the excellent crystal structure quality and the comparable chemistry allowed for bond and angle averaging within the s.u. at the 99% confidence level for many values. Thus, Table 3 presents averageable parameters drawn from all 17 structures. The atom numbering for C atoms used in this Table refers to the *first* 3,5-di*tert*butyl or the first phenyl ring in each structure, treating these rather different ring types separately, and can be keyed to the rings starting with C1 and C15 in Figure 2a. The source data for Table 3 is provided in Tables S4 and S5 (Supplementary information), wherein all the bond lengths and angles are reported for the individual structures grouped by these comparable geometrical categories. Full geometry data for each individual structure is provided in the archival CIF files. Comparisons of these results with the literature suggests that the geometries of each structure component is unexceptional, for example the selected bond lengths and angles agree with a previous phosphine bearing 3,5-*tert*butylphenyl groups.[14] Likewise, phenyl rings bearing 4-$OSi(CH_3)_3$ [30,45,46] and 4-OH [47-49] substituents are found to be comparable to those found in similar structures in the indicated literature.

Table 3. Averaged values of selected bond lengths and angles for the 17 structures. [a]

Averageable lengths	Length/Å [b]	Averageable angles	Angle/°[b]
S–P	1.961 (7)	C–P–S	113.5 (8)
Se–P	2.121 (6)	C–P–Se	113.1 (9)
O–P	1.501 (5)	C–P–O [c]	112.2 (11)
P–C (phosphine)	1.837 (3)	C–P–C (phosphine)	101.5 (10)
P–C (sulfide)	1.815 (7)	C–P–C (sulfide)	105.2 (11)
P–C (selenide)	1.815 (5)	C–P–C (selenide)	105.6 (12)
P–C (oxide)	1.803 (6)	C–P–C (oxide)	105.9 (12)
C–O (phosphine)	1.374 (6)	C–C–O (4-OSi(CH_3)$_3$)	119.5 (4)
C–O (sulfide)	1.364 (5)	C–C–O (sulfide) [d]	122.0 (9)
C–O (selenide)	1.369 (6)	C–C–O (selenide) [d]	115.5 (7)
C–O (oxide)	1.372 (6)	C–Si–O	110.2 (8)
Si–O	1.661 (5)	C–O–Si (phosphine)	142.0 (6)
Si–C	1.863 (9)	C–O–Si (S and Se)	147.4 (5)
(C1–C2), (C1–C6)	1.394 (4)	C–Si–C	111.0 (6)
(C2–C3), (C5–C6)	1.404 (10)		
(C3–C4), (C4–C5)	1.407 (12)		
^{t}*Bu* C–C (aromatic ring)	1.541 (3)		
C–C (-(CH_3)$_3$ ^{t}*Bu*)	1.539 (4)		
(C15–C16), (C15–C20)	1.397 (4)		
(C16–C17), (C19–C20)	1.393 (3)		
(C18–C19), (C17–C18)	1.390 (3)		

[a] Values presented in this table do not consider the minor components for the disorder model for **3**. The atom numbering is keyed to the rings starting with C1 and C15 in Figure 2a. [b] Errors are standard deviations of the indicated comparable values using the atom numbering schemes for the first ring of each kind. [c] Distance and angle values for **4c''** were removed due to incomplete oxidation. [d] Values for C–C–O for oxide structures (**2c**, **2c'**, **4c**, **4c'** and **4c''**) and for **2** and **4** are not shown because the H-bonds and/or intermolecular interactions influence these bond angles.

Phosphine **1** (Figures 2a, S1, S2) crystallizes in the space group $P2_1/n$ and approximates to what we will term a "flat" conformation, i.e., one of the three aryl rings is oriented orthogonal to a vector that contains the principal axis of the molecule through P and the nonbonded electrons on phosphorus, whilst the other two rings are strongly twisted towards being parallel to this vector. By contrast, phosphine **3** (Figures 2b and S9, also in $P2_1/n$) is in a close-to-helical conformation, in which all three aryl rings are oriented like propeller blades about the principal rotation axis of the trigonal pyramid. In our previous study, we found that these two conformations, flat and helical, were common for *tris*-(3,5-di*tert*butylphenyl)-phosphine derivatives or even coexist in a specific $Z' > 1$ unit cell.[14] Hybrid DFT calculations were performed at the B3LYP/6-31G(2d,p) level of theory and the computed flat geometries were found to be about 6 kJ·mol^{-1} higher in energy than the corresponding lowest-energy helical conformers. An optimization starting with the flat conformer smoothly converts to a helical geometry.[14] The former corresponds directly to Mislow's intermediate for the 'two-ring flip' mechanism for racemization of chiral, pyramidal Ar_3E molecules.[50]

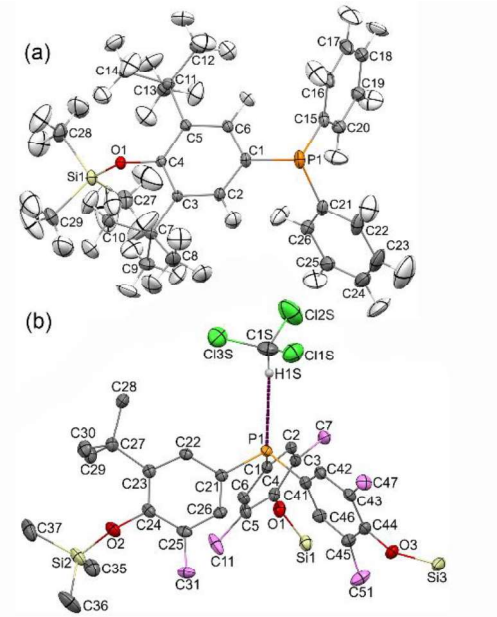

Figure 2 Displacement ellipsoid plots (50% probability) of the structures as found in their crystal lattices: (a) **1**, in the flat conformation (see text), and (b) **3**, in the helical conformation, showing the key atom labels. The short contact between P1 and solvent H1S in **3** is indicated by a dashed line. A second, disordered, molecule of $CHCl_3$ has been removed from the refinement model using a solvent mask. H atoms attached to C, methyl groups attached to Si1 and Si3 and to the pink-colored ^{t}Bu central C atoms C7, C11, C31 and C51, as well as the atoms of the minor components of the disorder to the C44-O3-Si3 siloxane group in **3** are omitted for clarity. For other views, see Figs. S1, S2, S9 and S10.

The $OSi(CH_3)_3$ group in the structure of **1** is oriented perpendicular to the plane of the aromatic ring and in the *endo* direction (on the side of the ring opposite to that of the P non-bonded electrons). A search of the Cambridge Structure Database, Release 5.42 with updates to Sep 2021 (CSD), located 70 examples for ∠benzene-O-$Si(CH_3)_3$ bond angles, with a mean value of 129.7 (7)°.[51] Thus, the angle in **1** is considerably larger at 142.42(3)°. However, restricting the comparison group to just 2,6-di*tert*butylphenyl-O-$Si(CH_3)_3$ derivatives, resulted in just 10 such bonds in the CSD, averaging to 140 (6)° and covering a very wide range from 126.8-150.3°, including two structures related to reagents used in this work (CSD refcodes: KUGMEH, KUGMAD).[30] Thus, there appears to be a significant steric effect on this bond angle from flanking *tert*butyl groups, but also considerable scope for flexibility in this parameter.

In the structure of phosphine **3**, the Si3 trimethylsiloxy group is positionally disordered (0.83:0.17 ratio) in concert with a placement disorder of a second $CHCl_3$ solvent molecule that is located just above the C41-C46 aromatic ring (s*ee Figures 2b and S10*). The major component of this siloxane is associated with a significant widening of ∠C44-O3-Si3, to 150.72(15)°, compared to ∠C44-O3A-Si3A, 146.8(1)°, or the ordered sites ∠C24-O2-Si2, 142.6(1)°, and ∠C4-O1-Si1, 141.28(1)°. (The whole of this second $CHCl_3$ has

been omitted in the final refinement with use of a solvent mask as part of the NoSpherA2 refinement strategy; see Experimental for details.) The structure of **3** has the two ordered $OSi(CH_3)_3$ groups oriented *endo* (as also seen for **1**) whilst the disordered substituent components are both oriented *exo*.

Phosphine **3** has a short *d*(P···H) = 2.66 (3) Å intermolecular interaction between P1 and the H1S of the refined (and ordered) chloroform molecule that is 0.340 < $\sum r_{vdW}$ (Table 4). Similar phosphorus-chloroform interactions are rare in the literature, with the CSD reporting six relevant cases with mean *d*(P···H) = 2.9 (1) Å, *d*(D···A) = 3.6 (3) Å and from 0.36 to 0.01 Å < $\sum r_{vdW}$. The most comparable structures to **3** have CSD refcodes: LOZSUR,[53] JEHSUH[54] and MOPXIA.[55]

Insert Table 4 near here.

Phosphine sulfide **3a** and selenide **3b** have solvent-free, ordered, isomorphous structures (Figures 3, S11-S13) in the trigonal space group *R*3*c*, occupying Wyckoff sites 6*a* with 3-fold rotation symmetry-precise helical conformations. Only one third of the molecules serve as the asymmetric units. Here, the $OSi(CH_3)_3$ groups are (all) oriented *endo*. Despite the structural variations amongst **1**, **3**, **3a** and **3b**, all their Si-O bond lengths and C-O-Si angles are extremely similar, averaging to 1.661 (5) Å and 142.0 (6)°, respectively (Tables S2 and S3). These interesting structures appear to be the first triarylphosphine derivatives possessing an $OSi(CH_3)_3$ ring substituent to have been deposited in the CSD.

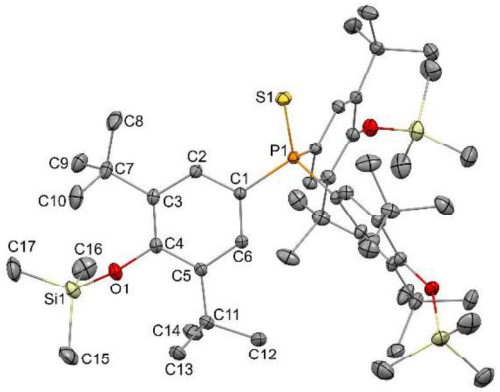

Figure 3 Displacement ellipsoid plot (50% probability) of structure **3a** as found in the crystal lattice, showing the atom numbering scheme for the asymmetric unit ($^1/_3$ of the molecule) in *R*3*c*. The structure shown is also valid for selenide **3b**. H-atoms on C omitted. For other views, see Figs. S11 and S12.

Figure 4a presents the structure of phosphine **2**, which crystallizes in monoclinic space group *I*2/*a*, approximates to the flat conformation, and is in general highly similar to that of the siloxane **1**, except that the OH group is effectively coplanar with the aromatic ring (compare Fig. 2a). Figure 4a also illustrates that *whenever* the flat conformation occurs, it involves a 3,5-di*tert*butyl-substituted ring and never a

simple phenyl ring. The structure refines extremely well using asymmetric structure factors computed by NoSpherA2, yielding R_1 = 2.60% and wR_2 = 7.18%, and is depicted with anisotropic displacement ellipsoids for all H-atom (see also FigureS3). The average C−C bond precision is a remarkable 0.0012 Å as determined by PLATON. Phosphine **4** (Figures 4b and S14) crystallizes in space group $P2_1/c$ with a helical conformation very similar to the siloxane analog **3** except that the phenolic OH groups are all co-planar; of these, one is oriented towards the P atom while the remainder point away from P.

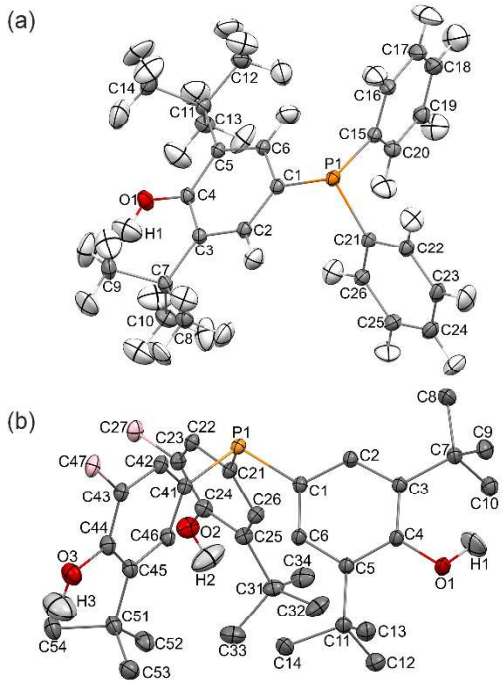

Figure 4 Anisotropic Displacement ellipsoid plot (50% probability) of all atoms in structures (a) **2** and (b) **4**, including atom numbering schemes. For clarity, H atoms attached to C and CH_3 groups attached to the pink-colored ^{t}Bu central C atoms C27 and C47 in **4** are omitted. For a full depiction of the H-atom treatments, see Figs. S3 and S14.

Noticeable in the crystal structures of phosphines **2** and **4** is the absence of expected hydrogen bonds involving the OH groups. This feature will be discussed below as one example of the *frustration of hydrogen bonding*. Another feature of **2** and all the other structures of phenols with flanking *tert*butyl groups are several significantly short intramolecular phenol OH to tertbutyl C–H contacts. A thorough computational investigation of these effects has recently been reported,[56] which are *inevitable* consequences of the steric crowding. The presence of these internal contacts has been implicated as contributing to the frustration of intermolecular H-bonding in such phenols.[23]

The phosphine sulfide and selenide structures **2a** and **2b** (Figures 5a and S4,6) are isomorphous in space group $P2_1/n$, and are fully ordered with no solvents in their lattices and approximate to the now-familiar flat conformations of the substituted aryl rings. In contrast, phosphine sulfide structure **2a'**

(Figures 5b and S5) occurs in $P\bar{1}$ and contains a disordered molecule of *m*-xylene in the crystal lattice; recourse was made to the solvent mask algorithm in Olex2 to remove the contribution of the solvent from the refinement model. Interestingly, **2a'** displays the lower-energy helical conformation for all the aryl rings and, consequently, the co-planar phenolic OH has an orientation; here it is directed up towards the P and S atoms. Despite such differences and disregarding the phosphorus sulfur/selenium bond length variations, the other distances and angles in structures **2a**, **2a'** and **2b** are indistinguishable (Table 3).

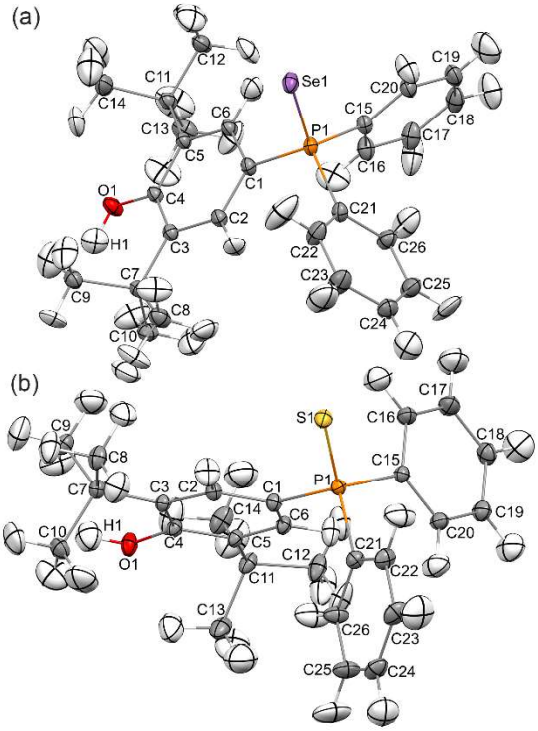

Figure 5 Displacement ellipsoid plots (50% probability) of (a) structure **2b** (and isomorphous sulfide **2a**); and (b) **2a'**, as found in their respective crystal lattices, showing the atom labeling scheme. Xylenes solvent has been removed from the refinement model of **2a'**. For other views, see Figs. S4, S5 and S6.

The crystal structure of **4a** (Figures 6a and S15) is unexpectedly isostructural with that of the parent phosphine **4** with only an increase in unit-cell volume of 4.4 % to accommodate the sulfur atom. Isostructural *tris*-(3,5-dimethylphenyl)-phosphine and its oxide, as well as *tris*-(4-methoxy-3,5-dimethylphenyl)-phosphine and its oxide are reported by Hill and Boeré,[57] so that there is precedent for this phenomenon. Phosphine sulfide **4a'** and selenide **4b** are isomorphous (Figures 6b, S16 and S17), also with a 4.4% increase in unit cell volume when Se replaces S; their lattices contain one molecule of xylenes per asymmetric unit. Since mixed isomers of xylenes were used to grow the crystals, it is unsurprising that the solvents appear to be disordered in the lattice. NMR spectra undertaken on crystals from the same batches as used for the diffraction experiments show xylene isomers in ratios 0.6(*m*):0.3(*p*):0.1(*o*) for **4a'**

and 0.4(*m*):0.4(*p*):0.2(*o*) for **4b**. Here too, solvent masks were employed to remove solvent contribution to the scattering densities (the resultant voids are then easily visualized). All selenide and sulfide structures derived from phosphine **4** have two co-planar phenolic OH groups pointed in the direction of the chalcogen, whilst the remainder are oriented in the opposite direction. Despite their differences, all phosphine sulfide and selenide structures (**2a**, **2a'**, **2b**, **4a**, **4a'** and **4b**) have a similar intermolecular interaction in the crystal lattice between the hydrogen of one of the OH groups and sulfur or selenium atoms (see below under Supramolecular Structures).

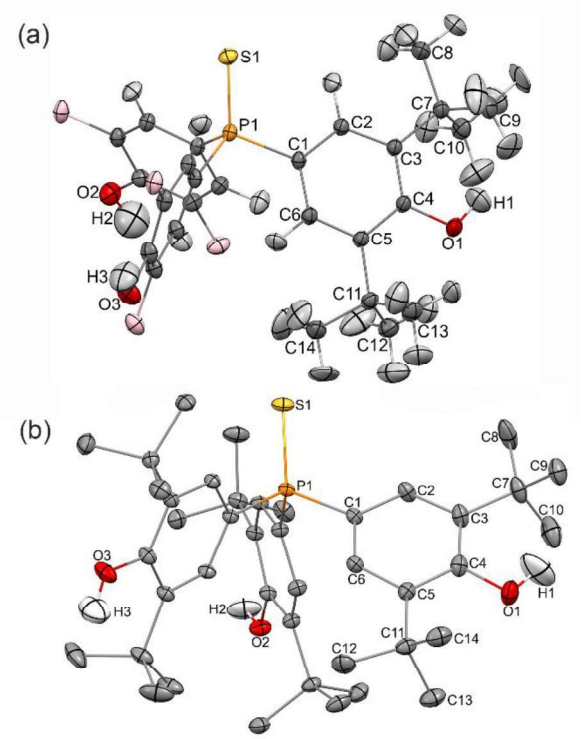

Figure 6 Displacement ellipsoid plot (50% probability) of structure (a) **4a** and (b) **4a'** as found in their crystal lattices. **4b** is isomorphous with **4a'**. For clarity only the first 3,5-di*tert*butyl-4-hydroxyphenyl atoms are labelled; the same sequence is used for the O2 ring starting with C21 and O3 ring with C41; CH_3 groups attached to the pink colored ^{t}Bu central C atoms in **4a**, H-atoms attached to C, xylene solvent, and a minor disorder component in **4a'** are omitted for greater clarity. For full H-atom treatments see Figs. S15 and 16.

In a statistical analysis, of 222 structures reported in the CSD for $Ar_3P{=}S$ where the aryl group is either phenyl or a substituted phenyl, the mean value for the P=S bond length is 1.952 (12) Å, whereas the mean *d*(P=S) value found in this project is 1.9607 (7) Å. A similar analysis on 78 $Ar_3P{=}Se$ structures returned a mean *d*(P=Se) value of 2.111 (13) Å, and the mean value in this work is 2.1210 (6) Å. In both cases, our results are well within range at the 99% confidence level, but are found in the upper quartiles of the comparison sets. Hence, the electron donating *tert*butyl, 4-$OSi(CH_3)_3$ and 4-OH substituents may

contribute to a slight elongation of P=S and P=Se distances. Amongst all the surveyed structures for P=S, only one has a 4-OR substituent (CSD refcode: ZEJLUV)[58], while for P=Se, three structures have this pattern (refcodes: ITEMOL[59], QAJZEI[39] and VIFJID).[60]

The two crystal forms of diphenyl-(4-hydroxy-3,5-di*tert*butylphenyl)-phosphine oxide that we obtained, structures **2c** and **2c'** (Figures 7a/S7 and 7b/S8, respectively), differ in that a disordered toluene solvent molecule is found in the **2c'** crystal lattice, which was removed from the refinement model using a solvent mask. The local molecular geometries are very similar, with almost ideal flat conformations of the substituted aryls and with phenyl rings that are both twisted by almost 90°. Whilst both were refined with the aid of NoSpherA2, **2c** is better defined than **2c'**, according to the expressed values of the mean bond precision: C-C= 0.0005 Å, R_1= 0.0104, wR_2= 0.0234 for **2c**, and bond precision: C-C= 0.0031 Å, R_1= 0.0597, wR_2= 0.1495 for **2c'**. Noticeable for both **2c** and **2c'**, the P atom is distorted (0.31 and 0.30 Å) above the 4-HO-3,5-di*tert*butylphenyl ring planes, whereas P is essentially co-planar with each phenyl ring. Also, in both structures, the phenolic OH group is oriented perpendicular to the plane of the aromatic ring. Since this distortion is much greater than found in **1**, **2** or **2a**, it is likely that the strong H-bonding between the upturned hydroxyls and O=P moieties on neighboring molecules contributes significantly to the distortion (see below under Supramolecular Structures).

For comparison of the P=O bond lengths, a CSD search of 938 Ar_3P=O was undertaken with exclusion of metal coordination or adducts at oxygen, of which 232 are of Ph_3PO itself, reflecting the popularity of using it as a co-crystallizing agent for a wide variety of compounds. With exclusion of 4 outliers in which the chemical identity of the chalcogen is suspect, a mean value with s.u. of 1.487 (16) Å is obtained. P=O bond lengths in **2c** of 1.4955 (2) and **2c'** of 1.498 (1) Å are well within the database range at the 99% confidence level but convincingly in the upper quartile of the comparison set.

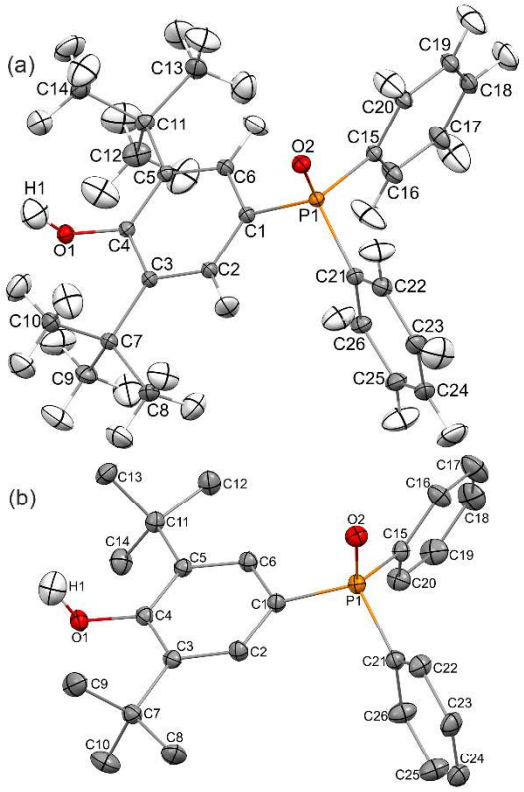

Figure 7. Displacement ellipsoid plot (50% probability) of the structure (a) **2c** and (b) **2c'** as found in their crystal lattices, showing key atom labels. Isotropically refined H-atoms are omitted for **2c'**. For other views see Figs. S7 and S8.

Three different structures of *tris*-(4-hydroxy-3,5-di*tert*butylphenyl)-phosphine oxide, here designated as **4c**, **4c'** and **4c''**, differ from each other in respect to crystal systems, space groups, conformations and the co-crystallized solvents. Structure **4c**, a monohydrated adduct containing a disordered water molecule, crystallizes in $P\bar{1}$ and has a helical conformation (Figures 8a and S18). By contrast, **4c'** (Figures 8b and S19) adopts a flat conformation in *P*4/*n* and entrains a mixture of *n*-butanol and water solvents in solvent channels that do not interact with the main molecules. These crystals were isolated from a failed attempt to extend the *para* substituent chain by alkylation at the phenol. The solvent was identified and removed from the refinement model using a solvent mask. The molecular conformation in this structure is very similar to that found in structures **2c** and **2c'**, despite the significant exchange of two C_6H_5 rings for 4-HO-3,5-(^{t}Bu)$_2$C$_6$H$_2$.

Crystal of **4c''** (Figures 8c and S20), obtained directly from the reaction mixture used for the chemical oxidation in acetone solutions, contain two co-crystallized solvent acetone molecules, and crystallizes in $P\bar{1}$. The asymmetric unit contains two distinct molecular structures, one (O4P1) with a helical, the other (O8P2) with a flat conformation. In structure **4c"**, both P=O refine to less than full oxygen occupancies, O4

at 89% and O8 at 70%. This implies that the phosphine was not fully oxidized by H_2O_2 at the time these crystals formed. Incomplete oxidation creates uncertainty in some bond lengths and angles in **4c''** (and are thus omitted from our average values) but the structure has been retained in this report because of its fascinating H-bonding pattern.

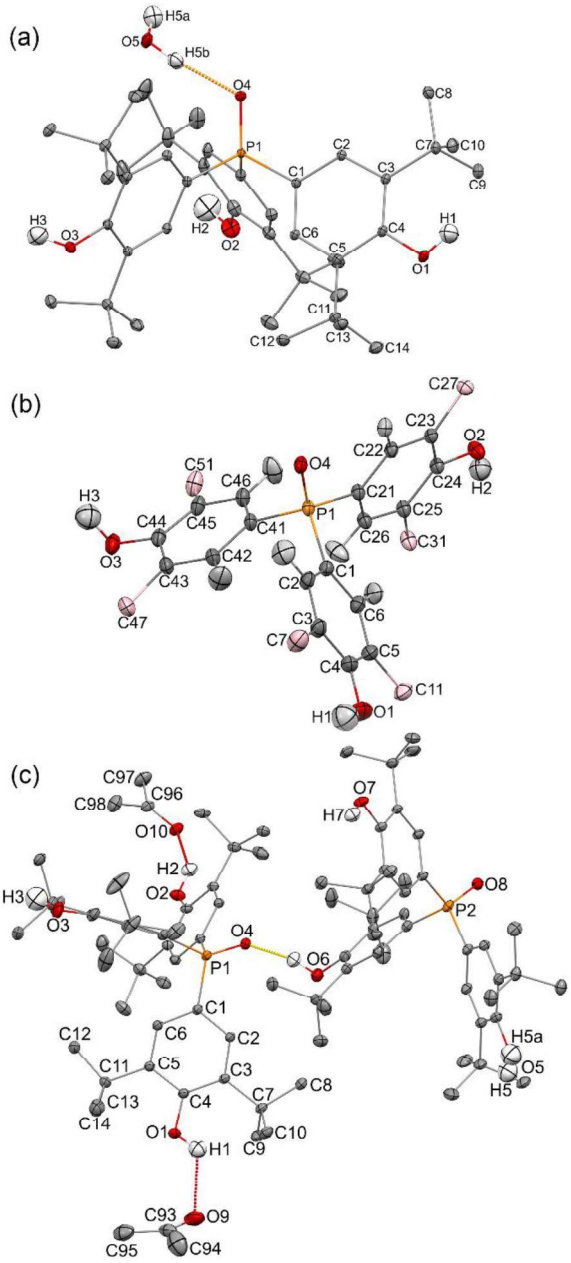

Figure 8 Displacement ellipsoid plots of structures (a) **4c** (30%), (b) **4c'** (50%) and (c) **4c"** (30% probabilities) as found in their crystal lattices. A disordered mixture of *n*-butanol and water has been removed from the refinement model of **4c'**. For clarity, the minor component of the disordered water oxygen (O5) in **4c** and acetone molecule (O9) in **4c''** have been omitted, as have H atoms attached to C in **4c** and **4c"**. CH_3 groups attached to the pink colored ^{t}Bu central C atoms are omitted in **4c'**, while only the first 3,5-di*tert*butyl-4-hydroxyphenyl and acetone atoms are labelled. H-bonds within the asymmetric units are shown by dashed lines. For full treatments of the H-atoms, see Figs. S18 - S20.

Whereas the P=O bong lengths of 1.5006 (5) and 1.509 (9) Å in **4c** and **4c'**, respectively, are indistinguishable from each other and from the results of the CSD P=O distances search (see above), and are both in the upper quartiles of the comparison sets, by contrast, the *d*(P=O) length values of 1.4732 (13) and 1.4477 (17) Å found for the two sites in **4c"** are significantly depressed from the partial oxygen occupancies and while within the statistical ranges at the 99% confidence level, are both in the lower ranges of the lowest quartiles. Results from this study and related work on phosphine oxides with bulky organic substituents [57] seems to indicate that database average P=O lengths may be underestimated from a significant degree of contamination by structures with *unrecognized* partial oxidation. Classic hydrogen bonds are "realized" in all these phosphine oxide structures (**2c**, **2c'**, **4c**, **4c'** and **4c''**), whilst **4c**, **4c'** and **4c''** *also* display partial frustration of H-bonding (details about the intermolecular interactions are described in the following section). Noteworthy in the refinement model of **4c"** is that the single OH group that is not involved in any intermolecular short contacts is disordered 50:50 into H5 and H5A, both involved in internal short contacts to the *tert*butyl CH groups (see above for details).

Supramolecular structures and interaction contacts. The 17 crystallographic structures described above can be classified according to intermolecular interactions into 4 different categories: those with only dispersion-induced short contacts (**1**, **3**, **3a** and **3b**), which are not further discussed; those with frustration of H-bonding (**2**, **2a**, **2a'**, **2b**, **4**, **4a**, **4a'** and **4b**); those with only classic H-bonding (**2c** and **2c'**) and those with combinations of classic and frustration of H-bonding (**4c**, **4c'** and **4c''**).

"Frustrated" $R_2^2(4)$ contacts. Phosphines **2** and **4** form dimers through very similar short contact interactions that do not fit the classic H-bonding definition (see below). Figure 9 presents the unusual H1–-O1$\cdots^{i/ii}$H1–O1$^{i/ii}$ (sym codes i: 1-*x*,1-*y*,2-*z* for **2** and ii: 1-*x*,-*y*,1-*z* for **4**) 'double embrace' between pairs of phosphines **2** and **4**, which is represented by graph set $R_2^2(4)$ [using Etter's notation].[62] The $R_2^2(4)$ contacts in **2** are characterized (Table 4) by *d*(D–A) = 3.0243 (12) Å, a long H$\cdots$A contact of 0.11 Å < $\sum r_{vdW}$, and by an acute ∠D–H–A of 107.9 (13) °. The similar interaction found in structure **4** is only marginally stronger as shown by *d*(H$\cdots$A) = 0.21 Å < $\sum r_{vdW}$.

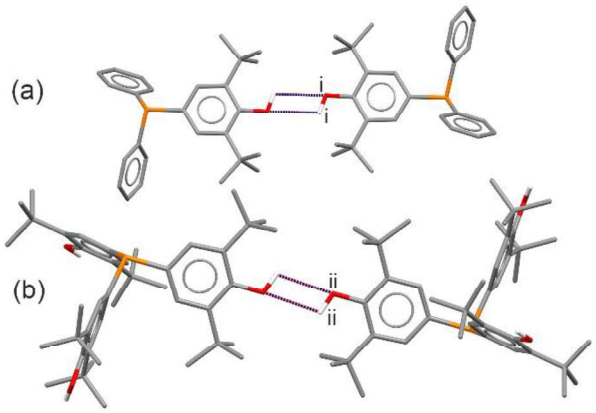

Figure 9 Stick diagrams depicting $R_2^2(4)$ intermolecular contacts in (a) **2** (sym code i: 1-*x*,1-*y*,2-*z*) and (b) **4** (sym code ii: 1-*x*,-*y*,1-*z*). H-atoms bound to C have been omitted.

Additionally, in phosphine **4** (Figure 9b) only one of three equivalent phenols, the O1H1 group, participates in the $R_2^2(4)$ dimer. By contrast, the O2H2 and O3H3 phenols lack any intermolecular interactions, participating only in intramolecular contacts to methyl CH units of the flanking *tert*butyl groups.[56] This represents a second type of frustration of H-bonding: the failure of such sterically shielded phenols to locate any suitable intermolecular acceptors. Since there is no structural distinction amongst them, a reasonable assumption is that both phenomena – complete frustration of contacts for O2H2 and O3H3 and unusually weak $R_2^2(4)$ contacts for O1H1 – have the same origin.

We agree with Lutz and Spek in a report on the structure of the parent 2,6-di*tert*butylphenol (CSD refcode: LERFET01) that these 'double embraces' do not qualify as classic H-bonds, and that the cause of this frustration of H-bonding is the steric shielding induced by the two flanking *tert*butyl substituents.[23] Yet as Etter has emphasized, phenols are both good proton donors and acceptors and thus are expected to be fully involved in H-bonding.[61,62] It is this contradiction that suggests the inclusion of such $R_2^2(4)$ contacts with the frustration of hydrogen bonding. Symmetric pairing occurs where structurally possible, but the energy of the interactions is insufficient to induce a lower density lattice which could enable all three available donors to participate in pairing simultaneously. Moreover, the donor-acceptor *d*(O···O) in each of **2**, **4** and **4'** (see below for **4'**) are shorter than the 3.1008 (11) Å in LERFET01.[23] Thus, while the geometries of these $R_2^2(4)$ interactions fail standard criteria, particularly the acute O–H···O angles (104.2 (13) - 107.9 (13)° in **2**, **4** and **4'** or 117.3 (16)° in LERFET01), the contact distances fall within the range for conventional electrostatic-covalent H-bonds.[21,22] A search of the CSD reported 617 structures containing the 2,6-di*tert*butylphenol entity. Searches out to a *d*(O···O) of 3.50 Å yielded only 66 results for contact pairs, indicating that 90% of such phenols do not form self-contacts. Next, a search restricted to *d*(O···O) of 3.05 Å or less, i.e. out to the sum of the van der Waals radii for two oxygen atoms, was undertaken,

and this still resulted in 20 hits. To ascertain what occurs at such short distances (including our results), the identified contacts were analyzed and are presented in Table 5. Contacts as short as 2.79 Å are amongst the set, though most are longer, averaging to 2.94 (6) Å (of course, this 'mean' is arbitrary, since it depends on the cutoff employed for the search). The ∠O–H···O angles cover a large range and may be affected by automated placements of, and varying abilities of the data to resolve, H atoms. Two general motifs were detected (Figure 10): in centrosymmetric pairs (including **2**, **4** and **4'**) the rings approach parallel and with in-plane OH groups in a 'double embrace' but may be vertically offset between 0 and 1.6 Å, and laterally offset (clearly visible in Figure 9a) from 0 to 0.8 Å; 13 of the 23 cases in Table 5 have this relationship through $\bar{1}$. Another five structures are related by a perpendicular 2-fold rotation axis, and these all have a twisted approach of the two aryl rings, ranging from 60 to 76°; twisting is also observed in a further three structures which have no symmetry constraints, whereas two of the unconstrained contact pairs adopt the offset parallel geometry typical of the $\bar{1}$ cases. A few of the twisted geometries also have mild bending about the C–O axes of the individual molecules. In view of this geometric specificity and the unusually short contact distances, (the stronger range of) such diphenol embraces are possible supramolecular synthons for 2,6-di*tert*butylphenol moieties. It is to be expected that there are multiple contributions to the interaction energies, including the OH dipoles but also dispersive attraction operating between the closely engaged *tert*butyl groups (Figure 10, right).

Insert Table 5 near here

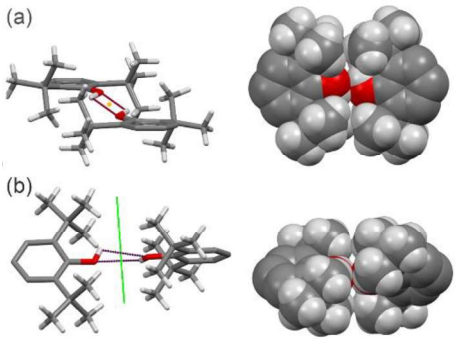

Figure 10. Two motifs for the phenol OH···OH 'double embrace'. 'Stick' (left) and (right) spacefilling representations of (a) $\bar{1}$ (yellow dot) and (b) ⊥2 (green line) interaction symmetries.

Reported triarylphosphine structures which have three 4-OH groups are extremely rare. A phosphine coordinated to iridium (CSD refcode: UXAQAM) contains three such substituents. One participates in $C_1^1(11)$ chains to benoxazolyl co-ligand O atoms in adjacent metal complexes, while H-bonding is frustrated for the other two phenol groups.[79]

'Redirected' $C_1^1(8)$ intermolecular contacts to weak acceptors. Phosphine sulfide and selenide structures **2a**, **2a'**, **2b**, **4a**, **4a'** and **4b** have similar intermolecular interactions involving the congested phenol donor regardless of whether the acceptor is a sulfur or selenium atom (Figures 11 and 12; Table 4), while the OH groups remain in the planes of their aromatic rings. These interactions give rise to infinite chains described by $C_1^1(8)$ graph sets, as illustrated in Figure 11a for **2b** (and isomorphous **2a**) which form helixes of period 2 along the *ac* unit cell direction and are symmetry related to parallel chains via the *n* glide $\perp$ to *b*. The otherwise very similar chains linked by OH···S contacts in **2a'** (Figure 11b) are in-register with period 1 and aligned along the crystal *a* axes. Parallel chains here are centrosymetrically related, as expected in $P\bar{1}$, since both molecules in the unit cell are part of separate chains. All these contacts appear to be stronger than the OH···HO 'double embraces', as judged from H···A distances that are 0.34 - 0.38 Å < $\sum r_{vdW}$. Moreover, the ∠O−H···A are less acute at 129 - 132°.

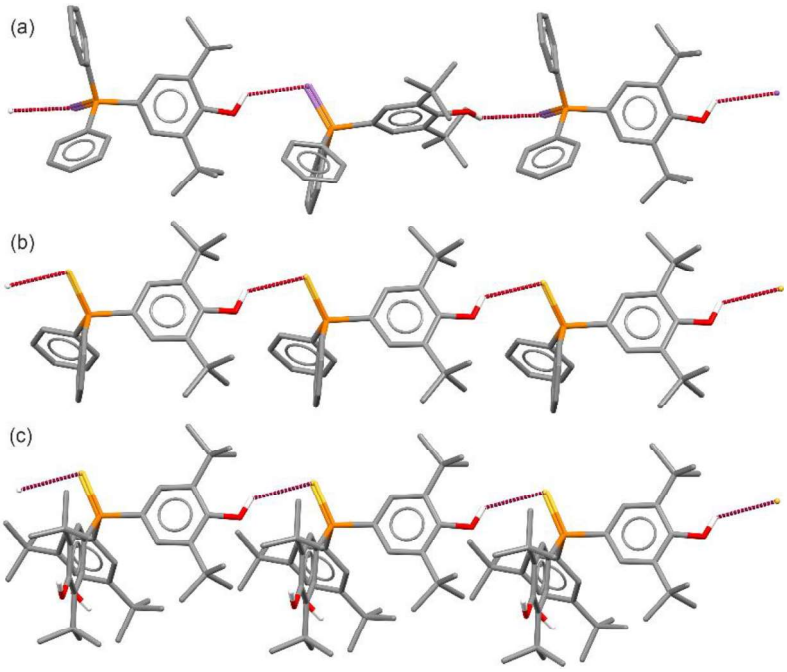

Figure 11 Stick diagrams depicting $C_1^1(8)$ intermolecular contacts in (a) **2b**, (b) **2a'** and (c) **4a'**. H-atoms bound to C have been omitted.

For **4a'** and isomorphous **4b** (Figure 11c), the phenol OH···E contacts (involving O2H2) form a series of extended chains along the crystal *a* axes with each molecule in the unit cell participating in a different chain. These chains have a period of 1 so that each monomer is replicated in its exact conformation, unlike the helical pattern observed for **2b**. Noticeably, the remaining phenols (O1H1 and O3H3) are unable to participate in any kind of intermolecular interactions. The *d*(OH···E=P) are 0.28 - 0.29 Å < $\sum r_{vdW}$ but the ∠O−H···A are larger at 136°. The observation in all these structures of apparently preferential H donation

to sulfur or selenium seems to be a result of *more accessible acceptors* in the phosphine sulfides and selenides; but as selenium is not considered an H-bond acceptor we also refrain from categorizing these as classic H-bonds. Here too, severe steric shielding of these 2,6-di*tert*butyl phenols results in an alternate intermolecular contact type in place of the expected OH···H hydrogen bonds.

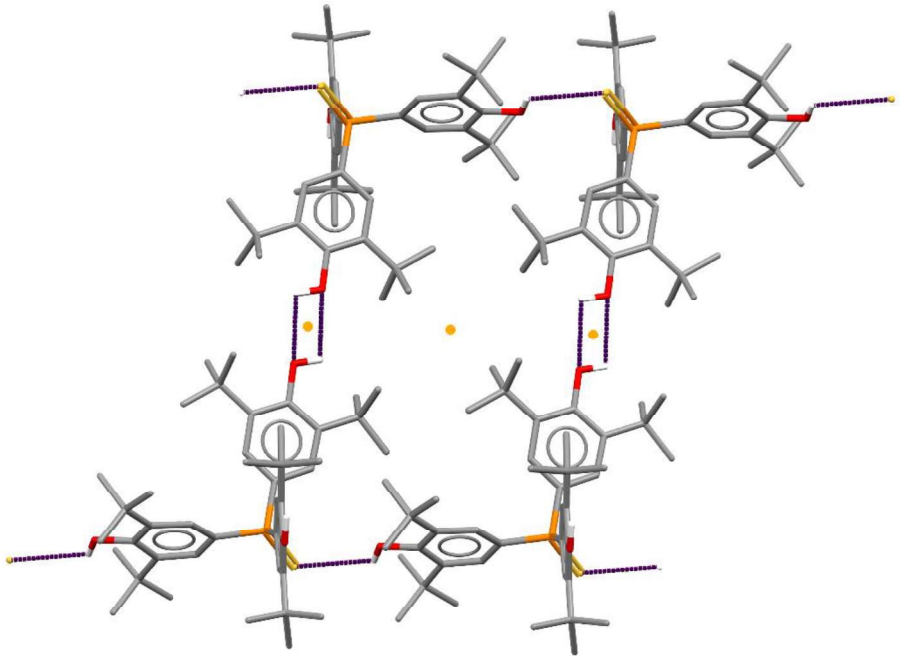

Figure 12. Stick diagrams depicting intermolecular contacts in **4a**. H-atoms bound to C have been omitted. Combinations of $C_1^1(8)$ links through the phosphine sulfide and centrosymmetric $R_2^2(4)$ phenol embraces describe the large level 2 $R_4^4(40)$ graph set. Inversion centers, $\overline{1}$ are shown as yellow dots.

The intermolecular contacts in **4a** in space group $P2_1/c$ (Figure 12) consist of an interesting combination of $C_1^1(8)$ O3H3···S=P chains, as in **2b**, **2a'** and **4a'**, with dimer-forming $R_2^2(4)$ phenol 'double embraces' of the type observed in **2** and **4** involving O1H1. The resulting $R_4^4(40)$ rings are centrosymmetric and extend via further $C_1^1(8)$ links into ribbons extending along the *a* axis and forming layers that are perpendicular to the *c* axis. The layers are then related to each other via the lattice *c* glide planes. This is a very interesting supramolecular architecture based on the two types of interactions so far encountered in this work. Nevertheless, short contacts involving the O2H2 phenols are frustrated by the apparent inability to find suitable acceptors amongst the atoms of the layers above and below the ribbon segment shown in Figure 12. In this structure, the O–H···S distance is only 0.15 Å < $\sum r_{vdW}$ with ∠O3−H3···S1 only 117°, and *d*(O1H1···H1) is 0.14 Å < $\sum r_{vdW}$ with ∠O1−H1···O1 = 104°, all indicative of weak interactions but sufficient in aggregate to organize the ribbon architecture.

Realized H-bonding with phosphine oxide acceptors. Classical hydrogen bonds characterized by a strong interaction between the H atom of the OH group and oxygen of the P=O are observed in the structures of phosphine oxides **2c** and **2c'** (Figure 13) The infinite H-bond chains in structures **2c** and **2c'** have extremely similar morphologies, even though **2c'** co-crystallizes with a disordered toluene molecule, the removal of which from the refinement model leaves large solvent voids in the crystal lattice. In both structures, helical $C_1^1(8)$ chains form that surround 2_1 screw axes and are therefore parallel to the crystal *b* axes of both lattices. The chain shape and dimensions are virtually identical and are defined by a strong supramolecular H-bonding motif, with H···O distances 0.91 – 1.1 Å < $\sum r_{vdW}$ and ∠O–H···O 173 – 132° (Table 4) that are well within the expected ranges for standard covalent-electrostatic H-bonds (see Table S1, Supporting Information).[20,22] Noticeably, the unit cell volume of **2c'** is some 13% larger to accommodate the solvent, whereas **2c** crystallizes solvent free. The chief structural effect of solvent inclusion or exclusion is that parallel chains are more tightly interdigitated in unsolvated lattice **2c** than in the solvated **2c'**, where toluene fills gaps induced by π-stacking between phosphine oxide phenyl rings and the aromatic solvent molecules (as determined from refinements in the IAM in which the solvent is retained).

Bis-(3,5-di*tert*butyl-2-hydroxyphenyl)-phenyl phosphine oxide (CSD refcode: QARXEM) reported by Siefert et al.[80] has two *intramolecular* hydrogen bonds from OH to P=O of the same magnitude as those observed for **2c** and **2c'** (D···A distances of 2.645 and 2.638 Å).

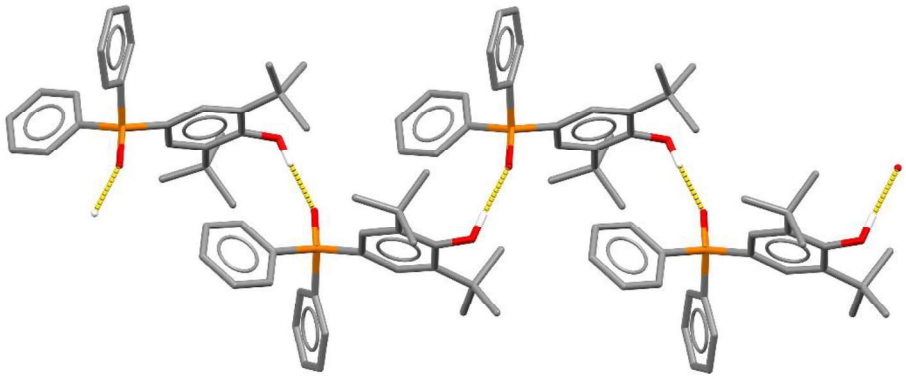

Figure 13. Stick diagrams of structure **2c** depicting classic H-bonds forming $C_1^1(8)$ graph sets. H-atoms bound to C have been omitted. The chain morphology found in **2c'** is effectively identical.

A notable feature of both **2c** and **2c'** is that the phenolic OH is rotated perpendicular to the 3,5-di*tert*butylphenyl planes (compare Figure 7 and Table 4), which results in a distinctly different, denser, chain morphology to those found in **2b**, **2a'** and **4a'**, although both types are described by $C_1^1(8)$ graph sets. A reasonable hypothesis for this difference in orientation is that co-planar is the most stable conformation for the OH group (by maximizing mesomeric bonding between the O non-bonded electrons

and the aromatic ring) [81] but that a sufficiently strong H-bond induces the perpendicular orientation because this gives much better access to the $^{-}$O–P^{+}Ar$_3$ acceptor. DFT calculations on conformers of **2c** (see S3 in Supporting Information) indicate that the perpendicular OH orientation is about 14 kJ·mol^{-1} higher in energy; classical H-bonds of the covalent-electrostatic type have energies in the range of ~17-63 kJ/mol.[21,22] Thus, it takes a considerably better H-bond acceptor, the phosphine oxide, to realize 'normal' hydrogen bonding for the phenolic OH group; such bonds can evidently supply sufficient energy to pivot the OH group to a geometry that enhances the interaction.

This perpendicular OH motif with classic H-bonding is also observed in the phosphine oxide structures **4c**, **4c'** and **4c''**, though not exclusively. Donation occurs to $^{-}$O–P^{+}Ar$_3$ acceptors but also to more standard acceptors water and acetone in these structures. For example, in the phosphine oxide monohydrate structure **4c** (Figure 14), upturned phenol O3H3 donates to water oxygen O5 as $D_1^1(2)$ pairs with *d*(H···O) 0.94 Å < $\sum r_{vdW}$ and ∠O–H···O of 157° (Table 4), in addition to conventional H-bonds between water and the phosphine oxide.

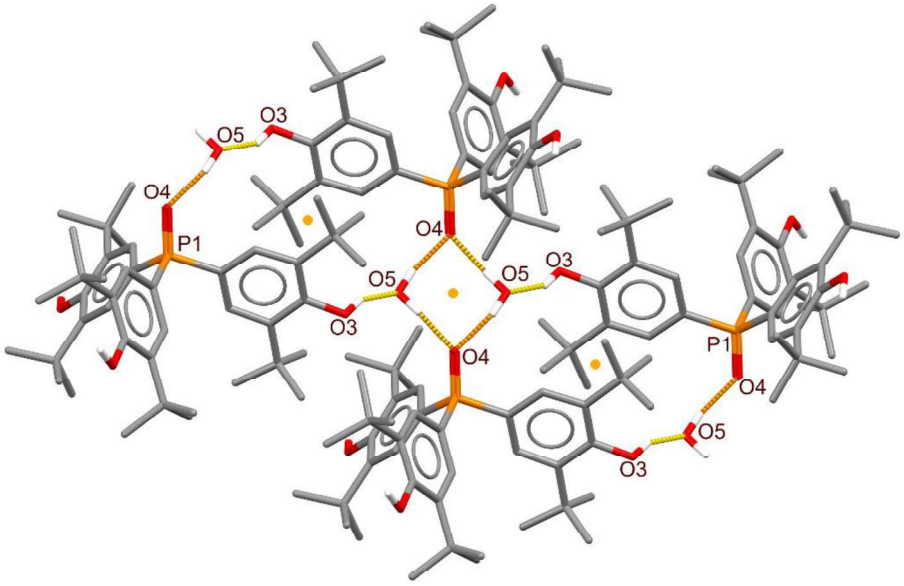

Figure 14. Stick diagrams depicting intermolecular contacts in structure **4c** in $P\overline{1}$. H-atoms bound to C have been omitted for clarity as has the minor component of disordered H_2O. The central $R_4^2(8)$ ring expands into the depicted larger $R_4^4(20)$ and $R_8^8(40)$ graphs. Yellow dots = $\overline{1}$.

The central H-bond graph set depicted in Figure 14 for **4c** is the $R_2^4(8)$ ring formed from two symmetry inequivalent H-bonds between the $^{-}$O–P^{+}Ar$_3$ acceptors and water donors with *d*(H···O) 0.78 – 0.87 Å < $\sum r_{vdW}$ and ∠O–H···O of 170 - 174°. In combination with the (stronger) $D_1^1(2)$ links to the phenol O3H3, larger rings are described such as the two $R_4^4(20)$ rings at top left and bottom right in Figure 14 and the

$R_8^8(40)$ net covering the whole figure. Extension of just these three independent H-bonds forms ribbons parallel to the *a* axis and perpendicular to the *bc* bisector. Yet, despite this very strong H-bonding and the presumed availability of additional water during crystallization, it is *only* the O3H3 phenol that is involved, leaving the O1H1 in the plane of the ribbons and O2H2 on the top/bottom of the ribbons phenols frustrated without significant intermolecular contacts.

Phosphine oxide structure **4c'**, which crystallizes in the tetragonal space group *P*4/*n*, does not show any molecular interactions of solvent (determined to be 50:50 *n*-butanol and H_2O) with the oxidized phosphine. The solvent is diffused along two channels parallel to *c* centred around the two 4-fold rotation axes in the unit cell and was removed from refinement using a solvent mask. H-bonded stacks of pure *tris*-(4-hydroxy-3,5-di*tert*butylphenyl)-phosphine oxide form in the unit cells around two crystallographic $\overline{4}$ rotoinversion axes in the unit cell; one layer of one such stack is depicted in Figure 15.

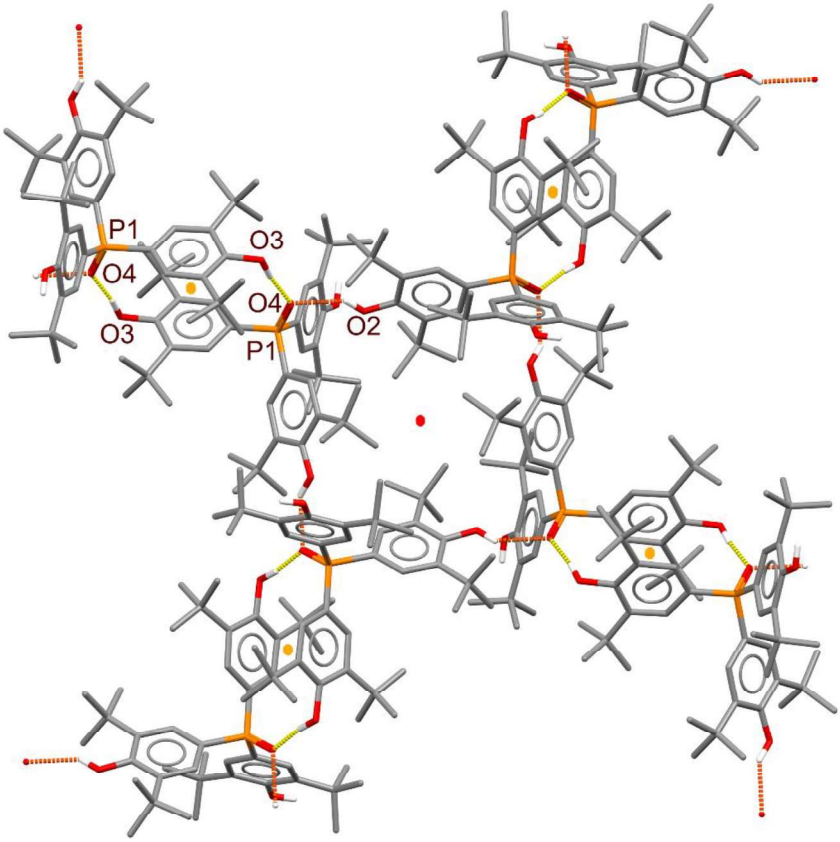

Figure 15. Stick diagrams depicting the structure of **4c'** in *P*4/*n*, described by a central $R_4^4(32)$ graph set that is surrounded by four $R_2^2(16)$ dimers through the bifurcated H-bonds to the $^-O–P^+Ar_3$. H-atoms bound to C have been omitted for clarity. The central red dot locates the (vertical) $\overline{4}$ axis and yellow dots = $\overline{1}$.

Only two symmetry-independent classic H-bonds create this extended network. The central level 1 $R_4^4(32)$ ring around the $\overline{4}$ axis is, fascinatingly, formed from the O2H2 phenol donor and the $^-O–P^+Ar_3$

acceptor, i.e. from an in-plane oriented phenol – the first occurrence of this 'mixed' motif. This bond is still relatively strong with an H···O distance that is 0.65 Å < $\sum r_{vdW}$ and an ∠O−H···O of 138° (Table 4). However, each acceptor participates in a bifurcated H-bond, accepting a second H more strongly (0.99 Å < $\sum r_{vdW}$ and ∠O−H···O = 172°) from the *out of plane* O3H3 phenol, forming a nested centrosymmetric dimer with another molecule that describes a level 1 $R_2^2(16)$ graph. Apparently, the perpendicular orientation of the phenol always leads to the strongest H-bonds, attributable to gaining better access thereby to the $^{-}O–P^{+}Ar_3$ acceptors.

The second molecule involved in each $R_2^2(16)$ dimer, at the four corners of the central tetragonal ring, bridges to the next such ring, and so this supramolecular architecture expands to an infinite layer in the *ab* plane of the lattice. These layers are perforated by the perpendicular, solvent-occupied, channels whose volume occupancy presumably enables this interesting architecture. Much larger level 2 rings surround the solvent channels, described simultaneously by $R_8^4(56), R_8^5(58), R_8^6(60), \text{and } R_8^7(62)$ graph sets. Apparently, the strong H-bonding that occurs *only* with itself in the **4c'** structure is robust enough to reject further interaction with *n*-butanol or water. Yet, even in this structure, H-bonding is entirely frustrated for the third phenol, the O1H1 case. These hydroxy groups are embedded amongst the *tert*butyl groups that define the hydrophobic boundaries between the infinite H-bonded layers lying perpendicular to the crystallographic *c* axis.

A phosphine oxide bearing three 2,6-diiodophenol rings (CSD refcode: WAMBOE), by contrast involves all three phenolic OH in H-bonding to DMSO and O=P acceptors.[82] This compound is a very close structural analog to **4c** as the flanking iodine atoms are large and in the same positions as the *tert*butyl groups. Specifically, a resemblance to part of the structure of **4c'** is observed as two of these molecules are also linked into a similar 'nested' $R_2^2(16)$ dimer. However, the remaining phenol OH groups in WAMBOE exclusively form pairwise H-bonds to the co-crystallized DMSO solvent molecules.

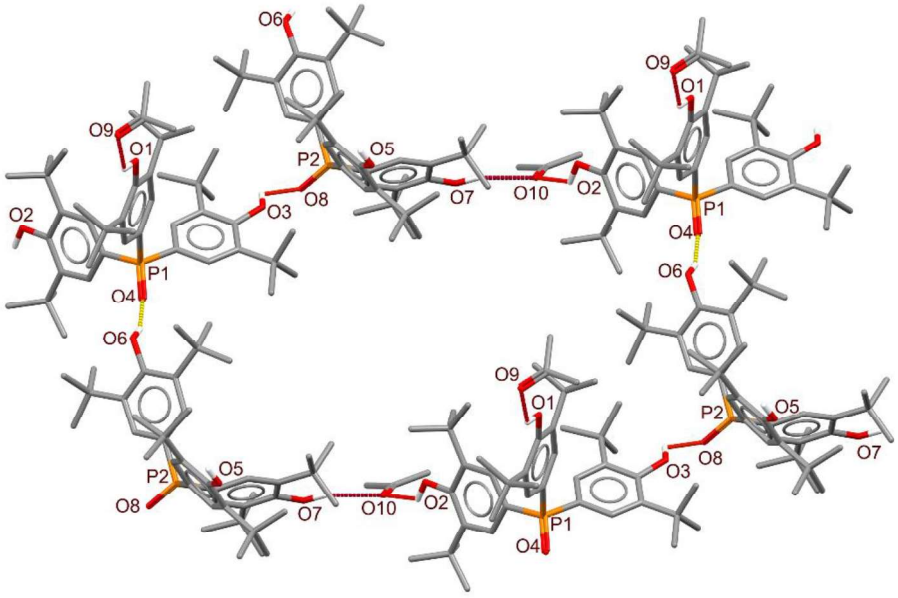

Figure 16. Stick diagrams depicting intermolecular contacts in **4c"**. H-atoms bound to C have been omitted for clarity. Eight molecules are linked via three acetones into a ring describing an $R_6^8(60)$ graph set.

The phosphine oxide network structure **4c"** depicted in Figure 16 consists of a large ring formed by eight H-bonds between the phenolic donors with, variously, $^{-}$O–P^{+}Ar$_3$ and O10 acetone acceptors, describing a level 4 $R_8^6(60)$ graph set. Additional terminal $D_1^1(2)$ H-bonds link O1H1 phenols to acetone O9 molecules (the 87% major component of a positional disorder). In all, three asymmetric units are involved, each including the two phosphine oxide molecules (P1: helical; P2: flat) and the two acetones (terminally linked O9, and bridging O10) – see also Figure 8c. This ring consists (clockwise, starting top left) of P1 molecules linked through O4P1 and O3H3, P2 via O8P2 and O7H7, O7H7···O10(acetone)···H2O2, P1 via H2O2 and P1O4, P2 via H6O6, P1 via H3O3 and O2H2, O2H2···O10(acetone)···H7O7, P2 via H7O7 and O6H6, completing the ring at O4P1. The entire network is described solely via the five kinds of H-bonds listed in Table 4, for which *d*(O–H···O) range from 0.34 – 0.96 Å < $\sum r_{vdW}$. Despite this abundance of H-bonding, interactions involving the O5H5/H5A phenol are frustrated from a lack of any accepting partners. Of the five realized phenol interactions, only O6H6 attached to one of the P2 rings is oriented perpendicular to its aromatic ring. As also seen in **2c**, **2c'**, **4c** and **4c'**, it is this perpendicularly oriented phenol that makes the strongest classical H bond. Indeed, across all the structures, bonds involving such 'upturned' phenols average to a *d*(D···A) = 2.66 (6) Å which are 0.99 (7) Å < $\sum r_{vdW}$. What is additionally significant from structure **4c''** is the strong confirmation that an in-plane phenol does not rule out classical H-bonding where suitable acceptors (O=P or O=C oxygen atoms) are available. However, such interactions (including the single case from **4c'**) seem to be weaker, with an average *d*(D···A) = 2.83 (6) Å which is 0.54

(8) Å < $\sum r_{vdW}$. The central hole in the large ring is partly filled by components of two neighboring rings, especially by additional O9 acetone molecules, but the H-bonded rings do not interlock.

On the accuracy of Hirshfeld Atom Refinement with NoSpherA2. Non-spherical atomic scattering factors were employed in all 14 structure models because of the importance of accurate locations of atoms involved in H-bonding.[18] This study was undertaken in part to test the utility and feasibility of using the recently developed NoSpherA2 code for calculating custom scattering factors on the fly. Whilst all the structures in this study were accurately determined using a fully modern diffractometer, and all reasonable precautions were taken to obtain good data, these structure determinations otherwise represent a normal cross-section from a synthetic chemistry project. The main concession towards optimizing the refinements was consistent use of Solvent Masking to remove the electron density associated with solvents not involved in H-bonding, so as to preserve data for use with the refinement of H-atoms positions and, where feasible, anisotropic displacement parameters. To ascertain the success of this approach, all C–H and O–H distances from these 14 structures were reviewed and the mean and s.u. data are compiled in Table 6. These HAR results compare favorably with a recent critical update of similar parameters obtained from neutron diffraction data, the acknowledged "gold standard" for accurate light-atom location in crystal structures (Table 6).[52]

Table 6. Mean Element Bond Lengths (Å) from NoSpherA2 X-ray Refinement and Neutron Diffraction

Bond type (100 K)	**Mean (s.u.) in this work**	**Mean (s.u.) in Allen** [a]
*tert*butyl C–sp^3–H	1.089 (3)	1.084 (13)
TMS C–sp^3–H	1.090 (22)	1.084 (13)
phenyl C(*ar*)–H	1.079 (3)	1.085 (9)
2,6-aryl C(*ar*)–H	1.081 (15)	1.085 (9)
C–O–H	0.95 (5)	0.99 (3)

[a] Neutron data from a critical review of the literature for experiments taken at 60 ≤ T ≤ 140 K. *Allen, et.al. (2010)[52].*

Attention was also paid to the average C–C bond precision as determined by PLATON for refinements undertaken with the IAM and with NoSpherA2/olex2.refine. The average improvement in precision over all 14 structures was 34.9%, and the range of improvement was from 11 to 69% (Table S2 and Section 5 in Supporting Information). A reasonable correlation was also found between this marker for improvement in precision and the lowering of the R_1 parameters for the refinements (Figure S22). All these markers, especially the excellent results presented in Table 6, demonstrate the overwhelming success of NoSpherA2 for the HAR of X-ray diffraction structures to high accuracy.

Conclusions

A closely-related series of triarylphosphines and their chemical oxidation products with O, S and Se have been synthesized and fully characterized herein in which at least one of the aryl groups are 4-hydroxy-3,5-di*tert*butylphenyls. These have significantly augmented the number of phosphines, and their chalcogen derivatives, with 4-OH substitution. The $Ar_3P{=}Se$ compounds have been used to establish a phosphine basicity scale by comparing $^1J_{P,Se}$ coupling constants with the HOMO energies from DFT computations, with excellent correlation. A careful analysis of intermolecular contacts involving the phenolic OH groups in these structures has confirmed earlier reports that self-interactions among them are not able to establish conventional H-bonds. Moreover, where multiply substituted, complete frustration of intermolecular contacts is observed for many of the OH groups. Nevertheless, distinct motifs of 2,5-di*tert*butylphenol self-interactions, in the form of OH···HO 'double embraces' occur and have been classified along with some 20 similar results from the crystallographic literature. When more accessible acceptors are available, such as S or Se attached to P(V), OH contacts redirect towards them. And when more polar, *stronger*, $O^-{-}P^+Ar_3$ acceptors are available, some very interesting conventional H-bonds are formed. The use of NoSpherA2 for HAR in these 14 structures has proven to be astoundingly successful. It seems that there is finally a robust, easily implemented tool that will bring custom, on-the-fly generated, realistic scattering factors into general crystallographic practice.

Experimental section

General methods: All solvents used for synthesis were reagent grade or better and were rigorously purified by standard procedures.[83] THF was dried by refluxing with Na/benzophenone while xylenes were dried by refluxing with Na. 4-Bromo-2,6-di*tert*butylphenol (Aldrich) was used as received. 2,6-di*tert*butyl-4-bromophenoxytrimethilsylane used as a precursor in the synthesis of **1** and **3** was synthesized as previously reported by Lucente-Schultz *et. al*.[84] and adapted by Marszaukowski *et. al*.[30] Phosphines **1**, **2**, **3** and **4** were prepared by modification of the original report of Pastor & Hessell.[16] All work with air-sensitive phosphines was conducted in a dry N_2 atmosphere using modified Schlenk and vacuum line techniques. Elemental analyses for C, H, N, S were performed with a Vario Micro-cube Elemental Analyzer. 1D (^{1}H, ^{13}C{^{1}H}, ^{31}P{^{1}H}) and 2D (^{1}H–^{1}H gCOSY,^{1}H–^{13}C gHSQC, and ^{1}H–^{13}C gHMBC) solution-phase NMR experiments were recorded on a Bruker Avance II, 300 MHz or Bruker Avance III HD, 700 MHz spectrometer, at probe temperature using, in general, 20 mg samples of complexes dissolved in $CDCl_3$, containing a trace amount of tretramethylsilane (TMS) that was used as an internal reference (0 ppm). Archival spectral data are presented in the SI.

Preparation of diphenyl-(3,5-di*tert*butyl-4-trimethylsiloxyphenyl)-phosphine – **1**

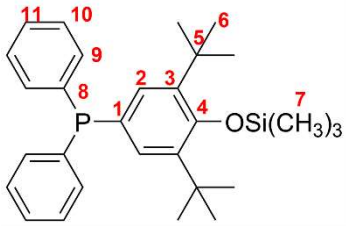

Synthesis of phosphine **1** was performed by adding 10.0 g (28.0 mmol) of 2,6-di*tert*butyl-4-bromophenoxytrimethilsylane in ~45 mL of dry THF in a 250 mL flask equipped with a side-arm stopcock, then cooled to -78 °C for 10 min with stirring. Then 36.2 mL (67.2 mmol) of commercial ^{t}BuLi was added dropwise and the resulting mixture was stirred for 1 h under N_2 atmosphere. After 1 h, 6.8 g (30.8 mmol) of chlorodiphenylphosphine was added dropwise. The resulting mixture was stirred for 30 min at -78 °C and then for 1 hour at room temperature. Unlocked NMR analysis indicated complete consumption of the starting material. After removing all volatiles to a vacuum trap, the residue was dissolved in ~150 mL of dry pentane which had been deoxygenated by Freeze-Pump-Thaw (FPT) and the resulting solution was stirred for 30 min. Thereafter, the suspension of lithium chloride was removed by filtration under N_2 atmosphere. Pentane was evaporated to a vacuum trap. Yield: 11.5 g (88.9%) pale yellow oil. M.P.: 63.2 – 64.2 °C; (dec. 106.7 °C). ^{1}H NMR (300.13 MHz, $CDCl_3$): δ H_7 0.33 (s, 9H, 3 CH_3); H_6 1.23 (s, 18H, 6 CH_3); H_2 7.12 (d, 2H, $J_{H\text{-}P}$= 8.3 Hz); $H_{9\text{-}11}$ 7.23 (m, 10H). ^{31}P{^{1}H} NMR (121.49 MHz, $CDCl_3$): δ -5.75, in good agreement with the literature values.[16]

Preparation of diphenyl-(3,5-di*tert*butyl-4-hydroxyphenyl)-phosphine – **2**

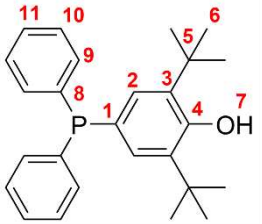

Synthesis of phosphine **2** was performed by aqueous hydrolysis of compound **1**. A solution of 11.5 g (24.9 mmol) of **1**, in ~20 mL of degassed methyl alcohol and 2 mL of degassed water in a 250 mL flask equipped with a side-arm stopcock was heated at reflux temperature for 4 h. The reaction was periodically monitored by unlocked NMR. When all **1** was consumed, the solution was cooled to room temperature and solvent was evaporated to a vacuum trap. After removing volatiles, the residue was quenched with 30 mL of H_2O which had previously been degassed by boiling under N_2, followed by 3 x 20 mL of CH_2Cl_2 which had been degassed by FPT. The organic phase (CH_2Cl_2 + phosphine) was transferred by canula to a clean flask containing anhydrous $MgSO_4$, the dried solution was filtered under N_2 atmosphere and then

volatiles were evaporated to a vacuum trap. Yield: 7.1 g (73.2%). M.P.: 89.5 – 90.5 °C; (dec. 112.7 °C). ^{1}H NMR (700.44 MHz, $CDCl_3$): δ H_6 1.27 (s, 18H, 6 CH_3); H_7 5.25 (s, 1H, OH); H_2 7.08 (d, 2H, J_{H-P}= 7.7 Hz); H_{8-11} 7.23 (m, 10H). ^{31}P{^{1}H} NMR (283.54 MHz, $CDCl_3$): δ -4.88. ^{13}C{^{1}H} NMR (176.12 MHz, $CDCl_3$): δ C_6 30.26 (s, 6 CH_3); C_5 34.48 (s, 2 C); C_1 125.64 (d, J_{C-P}= 5.45 Hz); C_{10} 128.34 (d, J_{C-P}= 2.33 Hz); C_{11} 128.34 (d, J_{C-P}= 2.33 Hz); C_2 131.32 (d, J_{C-P}= 22.19 Hz); C_9 133.49 (d, J_{C-P}= 18.87 Hz); C_8 135.90 (d, J_{C-P}= 7.74 Hz); C_3 138.52 (d, J_{C-P}= 10.55 Hz); C_4 154.86 (s, 1 C). C, H assignments confirmed by HSQC and HMBC. Elemental analysis calc. for $C_{26}H_{31}OP$ (%): C, 79.97; H, 8.00. Found: C, 80.01; H, 8.04.

Preparation of diphenyl-(3,5-di*tert*butyl-4-hydroxyphenyl)-phosphine sulfide – **2a**

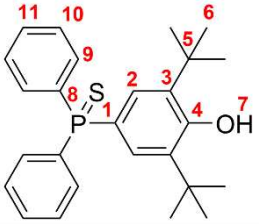

A 25 mL RB flask was charged with 300 mg (0.8 mmol) of compound **2** and 25.7 mg (0.1 mmol) of S_8 in 5 mL of dry xylenes. The solution was refluxed with stirring during 2 hours with periodic monitoring by unlocked NMR. When all **2** was consumed, the cooled solution was evaporated to dryness. The residue was dissolved in 5 mL of CH_2Cl_2, dried over anhydrous $MgSO_4$, filtered and solvent was evaporated. Yield: 201.0 mg, 61.8%. M.P.: 176.3 – 177.3 °C; (dec. 222.9 °C). ^{1}H NMR (700.44 MHz, $CDCl_3$): δ H_6 1.36 (s, 18H, 9 CH_3); H_7 5.59 (s, 1H, OH); H_{10} 7.43 (td, 4H, J_{H-H}= 7.0 Hz); H_{11} 7.48 (dd, 2H, J_{H-H}= 7.42 Hz); H_2 7.51 (d, 2H, J_{H-P}= 14.05 Hz); H_9 7.72 (m, 4H, J_{H-P}= 13.18 Hz). ^{31}P{^{1}H} NMR (283.54 MHz, $CDCl_3$): δ 43.75. ^{13}C{^{1}H} NMR (176.12 MHz, $CDCl_3$): δ C_6 30.07 (s, 6 CH_3); C_5 34.57 (s, 2 C); C_1 121.67 (d, J_{C-P}= 91.58 Hz); C_{10} 128.35 (d, J_{C-P}= 12.33 Hz); C_2 129.76 (d, J_{C-P}= 13.03 Hz); C_{11} 131.28 (d, J_{C-P}= 3.0 Hz); C_9 132.20 (d, J_{C-P}= 10.57 Hz); C_8 133.84 (d, J_{C-P}= 84.89 Hz); C_3 135.87 (d, J_{C-P}= 13.03 Hz); C_4 156.91 (d, J_{C-P}= 3.17 Hz).

Preparation of diphenyl-(3,5-di*tert*butyl-4-hydroxyphenyl)-phosphine selenide – **2b**

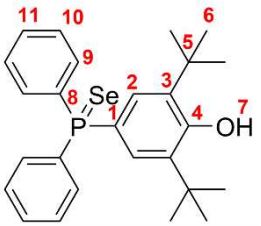

A 25 mL RB flask was charged with 300 mg (0.8 mmol) of compound **2** and 101.3 mg (1.3 mmol) of gray selenium in 5 mL of dry xylenes. The solution was refluxed with stirring during 2 hours with periodic monitoring by unlocked NMR. When all **2** was consumed, the cooled solution was evaporated to dryness. The residue was dissolved in 5 mL of CH_2Cl_2 and filtered through a plug of Celite™ to remove excess Se.

After filtering, solvent was evaporated to a vacuum line. Yield: 172.2 mg, 47.6%. M.P.: 201.2 – 202.2 °C; (dec. 222.9 °C). ^{1}H NMR (700.44 MHz, $CDCl_3$): δ H_6 1.36 (s, 18H, 9 CH_3); H_7 5.60 (s, 1H, OH); H_{10} 7.44 (td, 4H, J_{H-H}= 5.27 Hz); H_{11} 7.48 (m, 2H, J_{H-H}= 7.84 Hz); H_2 7.52 (d, 2H, J_{H-P}= 14.32 Hz); H_9 7.72 (m, 4H, J_{H-P}= 13.46 Hz). ^{31}P{^{1}H} NMR (283.54 MHz, $CDCl_3$): δ 35.45 (J_{P-Se}= 717.36 Hz). ^{13}C{^{1}H} NMR (176.12 MHz, $CDCl_3$): δ C_6 30.06 (s, 6 CH_3); C_5 34.60 (s, 2 C); C_1 120.38 (d, J_{C-P}= 83.30 Hz); C_{10} 128.37 (d, J_{C-P}= 12.50 Hz); C_2 130.22 (d, J_{C-P}= 13.21 Hz); C_{11} 131.32 (d, J_{C-P}= 3.00 Hz); C_9 132.57 (d, J_{C-P}= 10.74 Hz); C_8 132.78 (d, J_{C-P}= 76.61 Hz); C_3 135.86 (d, J_{C-P}= 13.03 Hz); C_4 156.95 (d, J_{C-P}= 3.34 Hz). Elemental analysis calc. for $C_{26}H_{31}OPSe$ (%): C, 66.50; H, 6.61. Found: C, 66.61; H, 6.67.

Preparation of diphenyl-(3,5-di*tert*butyl-4-hydroxyphenyl)-phosphine oxide – **2c**

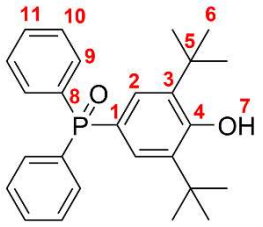

The synthesis was performed by dissolving 1 g (2.6 mmol) of compound **2** in 20 mL of acetone in a 50 mL RB flask. The solution was heating with stirring to reflux and 4% aqueous H_2O_2 (0.7 mL of 30% H_2O_2 diluted with 5mL of H_2O) was added dropwise. Then, the solution was refluxed with stirring during 2 hours with periodic monitoring by unlocked NMR. White crystals formed on cooling to RT, filtered, and dried under vacuum. Yield: 857.0 mg (85.4%). M.P.: 211.8 – 212.8 °C; (dec. 301.5 °C). ^{1}H NMR (700.44 MHz, $CDCl_3$): δ H_6 1.35 (s, 18H, 9 CH_3); H_7 5.64 (s, 1H, OH); H_2 7.40 (d, 2H, J_{H-P}= 12.83 Hz); H_{10} 7.44 (t, 4H, J_{H-H}= 7.58 Hz); H_{11} 7.52 (t, 2H, J_{H-H}= 7.35 Hz); H_9 7.68 (td, 4H, J_{H-P}= 8.26 Hz). ^{31}P{^{1}H} NMR (283.54 MHz, $CDCl_3$): δ 31.01. ^{13}C{^{1}H} NMR (172.12 MHz, $CDCl_3$): δ C_6 30.06 (s, 6 CH_3); C_5 34.47 (s, 2 C); C_1 121.53 (d, J_{C-P}= 112.19 Hz); C_{10} 128.35 (d, J_{C-P}= 11.98 Hz); C_2 129.52 (d, J_{C-P}= 12.15 Hz); C_{11} 131.71 (d, J_{C-P}= 2.29 Hz); C_9 132.10 (d, J_{C-P}= 9.86 Hz); C_8 133.03 (d, J_{C-P}= 104.97 Hz); C_3 136.03 (d, J_{C-P}= 12.68 Hz); C_4 156.79 (d, J_{C-P}= 3 Hz). Elemental analysis calc. for $C_{26}H_{31}O_2P$ (%): C, 76,80; H, 7.63. Found: C, 76.68; H, 7.69.

Preparation of *Tris-(*3,5-di*tert*butyl-4-trimethylsilyloxyphenyl)-phosphine – **3**

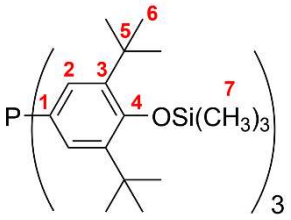

A solution of 12.0 g (33.6 mmol) of 2,6-di*tert*butyl-4-bromophenoxytrimethilsylane in ~40 mL of dry THF in a 250 mL flask equipped with a side-arm stopcock was cooled to -78 °C for 10 min with stirring. Then

37.8 mL (67.2 mmol) of commercial ^{t}BuLi was added dropwise and the resulting mixture was stirred for 1 h. After 1 h, 1.6 g (11.2 mmol) of PCl_3 was added over a further 10 min. The resulting mixture was stirred for 1 h at -78 °C and then for 30 min at room temperature. Unlocked NMR analysis indicated complete consumption of the starting material. After removing all volatiles to a vacuum trap, the residue was dissolved in ~150 mL of dry pentane which had been deoxygenated by sparging with N_2 and the resulting solution was stirred for 30 min. Thereafter, the suspension of lithium chloride was removed by filtration under N_2 atmosphere. Pentane was evaporated to a vacuum trap and the residue was triturated with acetonitrile to give 8.2 g (86.0%) of a white solid. M.P.: 166.6 – 167.6 °C; (dec. 216.1 °C). ^{1}H NMR (700.44 MHz, $CDCl_3$): δ H_7 0.39 (s, 27H, 9 CH_3); H_6 1.29 (s, 54H, 27 CH_3); H_2 7.09 (d, 6H, J_{H-P}= 8.4 Hz). $^{31}P\{^{1}H\}$ NMR (121.49 MHz, $CDCl_3$): δ -9.15, in good agreement with the literature values.[16] $^{13}C\{^{1}H\}$ NMR (176.12 MHz, $CDCl_3$): δ C_7 2.78 (m, 9 CH_3); C_6 30.29 (d, 27 CH_3); C_5 34.18 (t, 6 C); C_1 128.04 (s); C_2 130.47 (d, J_{C-P}= 14.09 Hz); C_3 139.39 (d, J_{C-P}= 4.74 Hz); C_4 152.66 (s). C, H assignments confirmed by HSQC and HMBC.

Preparation of *Tris*-(3,5-di*tert*butyl-4-trimethylsilyloxyphenyl)-phosphine sulfide – **3a**

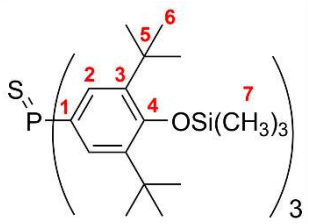

A 25 mL RB flask was charged with 200 mg (0.2 mmol) of compound **3** and 23 mg (0.1 mmol) of S_8 in 5 mL of dry xylenes. In all other respects the procedure was the same as described before for **2a**. Yield: 129.0 mg, 63.2%. M.P.: 198.3 – 199.3 °C; (dec. 211.7 °C). ^{1}H NMR (700.44 MHz, $CDCl_3$): δ H_7 0.40 (s, 27H, 9 CH_3); H_6 1.31 (s, 54H, 27 CH_3); H_2 7.48 (d, 6H, J_{H-P}= 14 Hz). $^{31}P\{^{1}H\}$ NMR (283.54 MHz, $CDCl_3$): δ 42.89. $^{13}C\{^{1}H\}$ NMR (176.12 MHz, $CDCl_3$): δ C_7 2.76 (s, 9 CH_3); C_6 30.06 (s, 27 CH_3); C_5 34.36 (s, 6 C); C_1 123.48 (d, J_{C-P}= 90.71 Hz); C_2 129.24 (d, J_{C-P}= 12.68 Hz); C_3 139.62 (d, J_{C-P}= 12.50 Hz); C_4 154.81 (d, J_{C-P}= 2.82 Hz). Elemental analysis calc. for $C_{51}H_{87}O_3PSSi_3$ (%): C, 68.45; H, 9.73; S, 3.58. Found: C, 68,47; H, 9,76; S, 3,61.

Preparation of *Tris*-(3,5-di*tert*butyl-4-trimethylsilyloxyphenyl)-phosphine selenide – **3b**

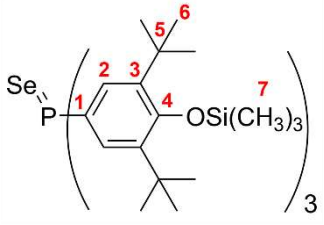

A 25 mL RB flask was charged with 200 mg (0.2 mmol) of compound **3** and 90.9 mg (1.2 mmol) of gray selenium in 5 mL of dry xylenes. In all other respects the procedure was the same as described before for

2b. Yield: 105.5 mg, 48.7%. M.P.: 217.6 – 218.6 °C; (dec. 255.4 °C). ^{1}H NMR (700.44 MHz, $CDCl_3$): δ H_7 0.40 (s, 27H, 9 CH_3); H_6 1.30 (s, 54H, 27 CH_3); H_2 7.48 (d, 6H, $J_{H\text{-}P}$= 14.00 Hz). ^{31}P{^{1}H} NMR (283.54 MHz, $CDCl_3$): δ 33.69 ($J_{P\text{-}Se}$= 700.91 Hz). ^{13}C{^{1}H} NMR (176.12 MHz, $CDCl_3$): δ C_7 3.79 (s, 9 CH_3); C_6 31.06 (s, 27 CH_3); C_5 35.41 (s, 6 C); C_1 123.41 (d, $J_{C\text{-}P}$= 82.77 Hz); C_2 130.61 (d, $J_{C\text{-}P}$= 12.85 Hz); C_3 140.64 (d, $J_{C\text{-}P}$= 17.26 Hz); C_4 155.88 (d, $J_{C\text{-}P}$= 2.82 Hz). Elemental analysis calc. for $C_{51}H_{87}O_3PSeSi_3$ (%): C, 65.04; H, 9.25; Found: C, 65.02; H, 9.57.

Preparation of *Tris*-(3,5-di*tert*butyl-4-hydroxyphenyl)-phosphine – **4**

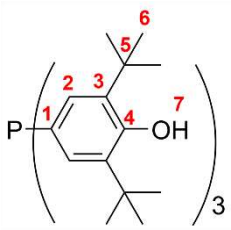

Phosphine **4** was obtained by aqueous hydrolysis of compound **3**. A solution of 8.2 g (9.5 mmol) of **1**, in ~20 mL of degassed methyl alcohol and 2 mL of degassed water in a 250 mL flask equipped with a side-arm stopcock was heated at reflux temperature for 4 h. The reaction was periodically monitored by unlocked NMR. When all **3** was consumed, the solution was cooled to room temperature and the white solid that precipitated was filtered under N_2 atmosphere and dried under vacuum. Yield: 3.8 g (61.3%). M.P.: 191.3 – 192.3 °C; (dec. 256.4 °C). ^{1}H NMR (700.44 MHz, $CDCl_3$): δ H_6 1.37 (s, 54 H, 27 CH_3); H_7 5.26 (s, 3H, 3 OH); H_2 7.13 (d, 6H, $J_{H\text{-}P}$= 7.70 Hz). ^{31}P{^{1}H} NMR (283.54 MHz, $CDCl_3$): δ -7.78. ^{13}C{^{1}H} NMR (176.12 MHz, $CDCl_3$): δ C_6 29.21 (m, 27 CH_3); C_5 33.42 (d, 6 C); C_1 127.02 (d, $J_{C\text{-}P}$= 5.81 Hz); C_2 129.66 (d, $J_{C\text{-}P}$= 21.31 Hz); C_3 134.45 (d, $J_{C\text{-}P}$= 7.22 Hz); C_4 153.19 (s). C, H assignments confirmed by HSQC and HMBC. Elemental analysis calc. for $C_{42}H_{63}O_3P$ (%): C, 77.98; H, 9.82; Found: C, 77.30; H, 9.85.

Preparation of *Tris*-(3,5-di*tert*butyl-4-hydroxyphenyl)-phosphine sulfide - **4a**

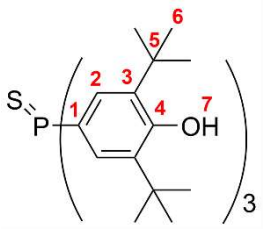

A 25 mL RB flask was charged with 200 mg (0.3 mmol) of compound **4** and 26 mg (0.1 mmol) of S_8 in 5 mL of dry xylenes. In all other respects the procedure was the same as described before for **2a**. Yield: 136.8 g, 66.5%. M.P.: 304.2 – 304.2 °C; (dec. 317.8 °C). ^{1}H NMR (700.44 MHz, $CDCl_3$): δ H_6 1.32 (s, 54H, 27 CH_3); H_7 5.51 (s, 3H, 3 OH); H_2 7.50 (d, 6H, $J_{H\text{-}P}$= 13.31 Hz). ^{31}P{^{1}H} NMR (283.54 MHz, $CDCl_3$): δ 43.40. ^{13}C{^{1}H} NMR (176.12 MHz, $CDCl_3$): δ C_6 29.07 (s, 27 CH_3); C_5 33.49 (s, 6 C); C_1 122.48 (d, $J_{C\text{-}P}$= 91.05 Hz); C_2

128.35 (d, $J_{C\text{-}P}$= 12.68 Hz); C_3 134.43 (d, $J_{C\text{-}P}$= 12.86 Hz); C_4 155.32 (d, $J_{C\text{-}P}$= 3.00 Hz). Elemental analysis calc. for $C_{42}H_{63}O_3PS$ (%): C, 74.34; H, 9.29; S, 4.73. Found: C, 74.32; H, 9.27; S, 4.81.

Preparation of *Tris*-(3,5-di*tert*butyl-4-hydroxyphenyl)-phosphine selenide – **4b**

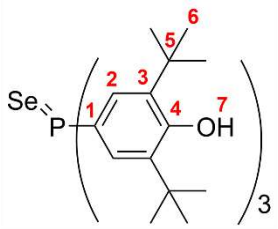

A 25 mL RB flask was charged with 200 mg (0.3 mmol) of compound **4** and 98.8 mg (1.3 mmol) of gray selenium in 5 mL of dry xylenes. In all other respects the procedure was the same as described before for **2b**. Yield: 123.1 g, 56.6%. M.P.: 306.8 – 307.8 °C; (dec. 312.4 °C). ^{1}H NMR (700.44 MHz, $CDCl_3$): δ H_6 1.36 (s, 54H, 27 CH_3); H_7 5.52 (s, 3H, 3 OH); H_2 7.50 (d, 6H, $J_{H\text{-}P}$= 14.00 Hz). $^{31}P\{^1H\}$ NMR (283.54 MHz, $CDCl_3$): δ 34.61 ($J_{P\text{-}Se}$= 698.93 Hz). $^{13}C\{^1H\}$ NMR (176.12 MHz, $CDCl_3$): δ C_6 30.08 (s, 27 CH_3); C_5 34.54 (s, 6 C); C_1 122.43 (d, $J_{C\text{-}P}$= 82.79 Hz); C_2 129.92 (d, $J_{C\text{-}P}$= 13.03 Hz); C_3 135.46 (d, $J_{C\text{-}P}$= 12.68 Hz); C_4 156.38 (d, $J_{C\text{-}P}$= 3.00 Hz). Elemental analysis calc. for $C_{42}H_{63}O_3PSe$ (%): C, 69.54; H, 8.69. Found: C, 69.83; H, 8.88.

Preparation of *Tris*-(3,5-di*tert*butyl-4-hydroxyphenyl)-phosphine oxide monohydrate – **4c**

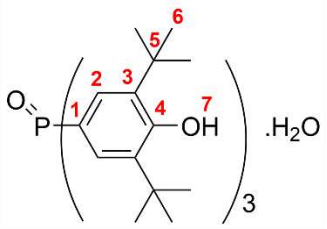

The synthesis was performed by dissolving 1 g (1.6 mmol) of compound **4** in 20 mL of acetone in a 50 mL RB flask. In all other respects the procedure was the same as described for **2c**. Yield: 918.0 mg (90.2%). M.P.: 254.8 – 255.8 °C; (dec. 301.3 °C). ^{1}H NMR (300.16 MHz, $CDCl_3$): δ H_6 1.38 (s, 54H, 27 CH_3); H_2O 1.85 (s, 2H); H_7 5.55 (s, 3H, 3 OH); H_2 7.43 (d, 6H, $J_{H\text{-}P}$= 12.60 Hz). $^{31}P\{^1H\}$ NMR (121.51 MHz, $CDCl_3$): δ 32.31. $^{13}C\{^1H\}$ NMR (75.48 MHz, $CDCl_3$): δ C_6 30.17 (s, 27 CH_3); C_5 34.49 (s, 6 C); C_1 123.36 (d, $J_{C\text{-}P}$= 109.75 Hz); C_2 129.46 (d, $J_{C\text{-}P}$= 11.70 Hz); C_3 135.55 (d, $J_{C\text{-}P}$= 12.45 Hz); C_4 156.66 (s). Elemental analysis calc. for $C_{42}H_{63}O_4P.H_2O$ (%): C, 74.08; H, 9.62. Found: C, 73.92; H,9.41.

X-ray crystallography: Single crystal X-ray diffraction experiments were undertaken using CuK_α (λ = 1.54184 Å) or MoK_α (λ = 0.71073 Å) radiation at 100 (1) K on a Rigaku-Oxford Diffraction SuperNova diffractometer equipped with a Pilatus P200 HPC detector. Suitable crystals of **1** and **2** were both obtained by dissolving the phosphines in hot heptane and then cooling them in a refrigerator. Crystals of **2a**, **2a'** and **2b** were obtained by dissolving phosphines in hot *m*-xylene and slow cooling to room temperature.

The same technique described above was used to obtain crystals of **2c** and **2c'** in acetone and toluene respectively. For **3** the crystals were obtained by adding a layer of acetonitrile over a saturated solution of the phosphine in chloroform at room temperature. Suitable crystals of **3a**, **3b**, **4a**, **4a'** and **4b** were obtained by heating/slow cooling of the solution in mixture of xylene isomers. Phosphine **4** crystals were obtained by slow cooling to room temperature from a methanol solution. Crystals of **4c**, **4c'** and **4c''** were obtained by heating/slow cooling in: solvent mixture 5:2 acetone/water, *n*-butanol and acetone, respectively. Crystals were coated in Paratone™ oil, mounted on a MiTeGen loop and cooled to 100 (1) K on the goniometer using the cold gas from an Oxford Cryostream 800. The images were integrated, the data processed and corrected for absorption using CrysAlisPro 1.171.38.43,[85] solved with SHELXT,[86] and refined by full-matrix LS minimization using SHELXL-2014[87] within the Olex2 suite of programs.[19] For all structures, further refinement using Levenberg-Marquardt minimisation was attempted with olex2.refine in conjunction with non-spherical atom scattering factors computed by NoSpherA2.[18] Quantum calculations to determine the electron density were undertaken with the ORCA program system, version 4.0, at the PBE/def2-TZVP level of theory.[88] A detailed description of the models developed using NoSPherA2 is provided in the Supporting Information.

Structures were visualized and analyzed using Mercury CSD Release 2021.2.0.[89] Crystal data and structure refinement details for all 17 structures are collected in Table 7 including the CSD Accession Codes. Selected averaged interatomic distances and angles are compiled in Table 3 and the original data in Tables S4 and S5 in the Supporting Information.

Quantum Computations: All computations were undertaken using DFT methods as implemented in the Gaussian W16 [90] program suite and interpreted using GaussView 1.6 [91] on personal computers equipped with 12-core Intel i7-8700 CPUs and 16 GB of RAM. The B3LYP-D3BJ/6-31+G(2d,p) level of theory was employed as a reasonable compromise between efficiency and speed so that the same level of theory could be applied uniformly from small molecules like triphenylphosphine and the largest cases, **3** and **4**. The latter took up to a month of wall time to converge. As previously recognized, the inclusion of dispersion is key to an accurate modelling of the pyramidality of aryl phosphines incorporating 3,5-di*tert*butylphenyl rings. The Grimme D3 [92] empirical dispersion model was adopted, with the inclusion of Becke-Johnston damping.[93] Although effective, the D3BJ method significantly slows convergence of these large, dispersion-enhanced substituted phosphines. Whenever possible, the achievement of at least local minima on the energy hypersurfaces were confirmed by frequency calculations with zero imaginary frequencies. For several of the phosphines listed in Table 2, multiple conformations could be optimized depending on the starting geometries. From these, the lowest energy conformers only were retained and

are listed in Table 2. Cartesian coordinates of all newly optimized molecules have been archived in the Supporting Information.

Associated Content

Supporting Information. The Supporting Information is available free of Charge at:

Additional Crystal Structure Graphics, DFT Computation – Further Details, Classification Table of Hydrogen Bond Types, 1D and 2D NMR Spectra, Further details on the X-ray Crystal Structure Determinations and Refinements, Archive of DFT Optimized Cartesian Geometries. A composite CIF file depicting all 17 crystal structures is also available.

Accession Codes. CCDC 201681, 2071684, 2072749–2072763 contain the supplementary crystallographic data for this paper. These data can be obtained free of charge via www.ccdc.cam.ac.uk/data_request/cif, or by emailing data_request@ccdc.cam.ac.uk, or by contacting The Cambridge Crystallographic Data Centre, 12 Union Road, Cambridge CB2 1EZ, UK; fax: +44 1223336033.

Acknowledgements

This work was underwritten by ongoing Discovery Grants from the Natural Sciences and Engineering Research Council (NSERC). The diffractometer at the University of Lethbridge X-ray Diffraction Facility was purchased by the University and the Faculty of Arts&Science. F.M. thanks the University of Lethbridge Research Fund for provision of a stipend for part of this work. The authors also thank the Brazilian agencies (CNPq PVE 401271/2014-5 and CAPES) for generous financial support through grants and scholarships. We are extremely grateful to Drs. Florian Kleemiß and Horst Puschmann of OlexSys Ltd. for generous support and discussion, especially with the early and less stable releases of NoSpherA2. Dylan J. Webb is acknowledged for undertaking the combustion analyses.

Table 2. Phosphine basicity from $^{1}J_{P,Se}$ of corresponding phosphine selenides and from DFT computation [a]

Parent phosphine	δ $^{31}P\{^{1}H\}$ Se=PAr$_3$	$^{1}J_{P,Se}$ (Hz) Se=PAr$_3$	HOMO energy (eV)	∑∠$_{CPC}$ ° of PAr$_3$ [b]	Dev ∑ ° [c]	pK$_B$ [d]	Ref.
4	34.61	698.9	-5.391	299.6	-4.5	7.0	this work
3	33.69	700.9	-5.389	298.3 [e]	-5.8	7.2	this work
(4-CH_3O-C_6H_3)$_3$P	31.50	711.0	-5.495	304.6	0.5	8.6	37
(4-CH_3O{3,5-CH_3}$_2C_6H_3$)$_3$P	32.74	711.4	-5.629	304.0	-0.1	8.6	38
({3,5-CH_3}$_2C_6H_3$)$_3$P	35.39	713.6	-5.744	304.1	0.0	8.9	38
(3,5-^{t}Bu$_2C_6H_3$)$_3$P (**A**)	34.54	714.0	-5.733	300.0	-4.1	8.9	34
2	35.45	717.4	-5.706	303.9	-0.2	9.4	this work
(4-$CH_3C_6H_3$)$_3$P	34.60	717.6	-5.758	304.4	0.3	9.4	39
2-CH_3O-$C_6H_3PPh_2$	32.80	718.0	-5.790	303.4	-0.7	9.5	40
(3-$CH_3C_6H_3$)$_3$P	34.70	720.2	-5.858	304.3	0.2	9.7	40
4-CH_3O-$C_6H_3PPh_2$	36.50	722.0	-5.791	304.6	0.5	10.0	41
Ph_3P	33.20	729.7	-5.992	304.5	0.4	11.0	42
(4-F-C_6H_4)$_3$P	34.50	740.0	-6.253	304.3	0.2	12.4	43
(4-$CH_3C{\equiv}CC_6H_4$)$_3$P	34.90	746.0	-6.116	304.4	0.3	13.2	44
(3-CF_3-C_6H_4)$_3$P	35.50	766.0	-6.757	303.7	-0.4	15.8	40
(3,5-{CF_3}$_2$-C_6H_4)$_3$P	33.90	802.0	-7.437	303.0	-1.1	20.5	44

[a] Calculations on geometry optimized structures at the B3LYP-D3BJ/6-31+G(2d,p) level of theory using Grimme's damped empirical dispersion correction, with frequency calculations to confirm true minima. [b] Geometries are taken from the DFT calculations to avoid complications with different conformations in crystal structures; the lowest-energy conformations were employed when more than one structure could be minimized. [c] Dev∑ = (∑∠$_{CPC}$ – mean), where the mean value over all but **3**, **4** and **A** is 304.1(5)°. [d] Using regression formula from Beckmann et.al. (2011)[37]. [e] This structure resisted full convergence and a frequency calculation was not obtained.

Table 4. Intermolecular Short Contacts and Hydrogen Bonds at 100 K

Comp.	D	H	A	d(D-H)/Å	d(H-A)/Å	< $\sum r_{vdW}$/Å	d(D-A)/Å	D-H-A/°	Contact Type	ArOH orient.
2	O1	H1	O2[1]	0.927(17)	2.607(18)	0.113	3.0243(12)	107.9(13)	ArOH···OHAr	in pl.
2a	O1	H1	S1[2]	0.939(12)	2.620(13)	0.380	3.2923(5)	128.9(9)	ArOH···S=P	in pl.
2a'	O1	H1	S1[3]	0.951(13)	2.601(13)	0.339	3.3130(6)	131.9(10)	ArOH···S=P	in pl.
2b	O1	H1	Se1[4]	0.93(2)	2.73(2)	0.370	3.3969(8)	129.5(14)	ArOH···Se=P	in pl.
2c	O1	H1	O2[5]	0.946(7)	1.805(7)	*0.914*	2.7498(4)	176.1(6)	Classic H-bond	*perp.*
2c'	O1	H1	O2[6]	1.09(4)	1.60(4)	*1.123*	2.681(2)	173(4)	Classic H-bond	*perp.*
3	C1S	H1S	P1	1.10(3)	2.66(3)	0.340	3.751(2)	173(2)	C–H···P	n/a
4	O1	H1	O2[7]	0.951(10)	2.516(11)	0.205	2.9196(9)	105.7(7)	ArOH···OHAr	in pl.*
4a	O1	H1	O1[7]	0.951(17)	2.582(18)	0.139	2.9622(14)	104.2(13)	ArOH···OHAr	in pl.[#]
	O3	H3	S1[9]	0.874(17)	2.846(19)	0.158	3.3388(8)	117.4(14)	ArOH···S=P	in pl.[#]
4'	O2	H2	S1[3]	0.937(13)	2.714(15)	0.287	3.456(7)	136.2(12)	ArOH···S=P	in pl.*
4b	O2	H2	Se1[8]	0.92(2)	2.82(2)	0.284	3.5315(10)	135.5(17)	ArOH···Se=P	in pl.*
4c	O3	H3	O5[9]	0.937(14)	1.767(15)	*0.953*	2.6570(8)	157.4(12)	Classic H-bond	*perp.**
	O3	H3	O5a[9]	0.937(14)	1.743(18)	*0.978*	2.568(11)	145.1(13)	Classic H-bond	*perp.**
	O5	H5a	O4[10]	0.925(16)	1.855(16)	0.865	2.7759(8)	173.7(13)	Classic H-bond	*water*
	O5a	H5a	O4[10]	1.006(19)	1.855(16)	0.865	2.576(12)	125.8(17)	Classic H-bond	*water*
	O5	H5b	O4	0.929(14)	1.940(15)	0.780	2.8591(8)	169.6(11)	Classic H-bond	*water*
4c'	O2	H2	O4[11]	0.887(14)	2.068(14)	0.652	2.7809(9)	136.7(12)	Classic H-bond	in pl.[#]
	O3	H3	O4[9]	0.970(16)	1.731(16)	*0.988*	2.6948(9)	171.6(14)	Classic H-bond	*perp.*[#]
4c''	O1	H1	O9[‡]	0.92(3)	2.29(3)	0.428	2.874(2)	121(2)	Classic H-bond	in pl.[†]
	O2	H2	O10	0.95(3)	2.20(2)	0.521	2.8931(15)	128.6(19)	Classic H-bond	in pl.[†]
	O3[‡]	H3	O8[12]	0.866(13)	2.15(5)	0.566	2.766(5)	127(5)	Classic H-bond	in pl.[†]
	O6	H6A	O4	0.91(3)	1.76(3)	*0.958*	2.6329(15)	158(2)	Classic H-bond	*perp.*[†]
	O7	H7	O10[13]	0.95(2)	2.38(2)	0.335	3.1368(15)	135.9(19)	Classic H-bond	in pl.[†]
Mean	All OH in list			0.939(43)	2.24(41)		2.98(33)	140(23)	Incl. short contac.	
Mean	ArOH···OHAr			0.943(11)	2.568(38)		2.969(43)	105.9(15)	"Frustrated"	
Mean	Classical HB			0.945(52)	1.94(23)		2.77(11)	147(19)	"Realized"	
Mean	Neutron data			0.989(27)[§]	—		—	—	60 ≤ T ≤140 K[§]	

Sym. codes: [1] 1-X,1-Y,2-Z; [2] 1/2+X,3/2-Y,-1/2+Z; [3] -1+X,+Y,+Z; [4] -1/2+X,3/2-Y,1/2+Z; [5] 1/2-X,-1/2+Y,1/2-Z; [6] 1-X,-1/2+Y,1/2-Z; [7] 1-X,-Y,1-Z; [8] -1+X,+Y,+Z; [9] 1-X,1-Y,1-Z; [10] 2-X,1-Y,1-Z; [11] 1-Y,-1/2+X,1-Z; [12] 1+X,+Y,+Z ; [13] X,Y,1+Z. Notes: Calculated by Mercury CSD (using Bondi van der Waals radii). * There are two additional in-plane ArOH with no interactions < $\sum r_{vdWaals}$. [#] There is one additional in-plane ArOH with no interactions. [†] One additional in-plane ArOH without interactions is 50:50 H-disordered. [‡] Disorder in O atom position affects accuracy. [§] Ref. Allen & Bruno, 2010[52] (excluding structures with very short intramolecular or very symmetrical H-bonds) – see original publication for details.

Table 5. Database Search of OH···HO Contacts in 2,6-di*tert*butylphenol Dimers

Structure (CSD refcode)	d(O···O)/Å	< $\sum r_{vdW}$ /Å[a]	∠O···HO/°	Symm.	Twist/°	Bend/°	Planar offset /Å	Lateral offset /Å	Ref.
XINQOD [b]	2.786	0.254	97.9	$2\perp$	64	175	0	0.17	63
REYNAN	2.827	0.213	111.4	$\bar{1}$	0		0.97	0.65	64
GIWTAH	2.828	0.212	99.5	none	37	170	0	0	65
KERCER	2.878	0.162	87.5	$2\perp$	62	171	0	0	66
ZOLNUM	2.915	0.125	90.9	none	0		0.37	0.44	67
4	2.9196(9)	0.120	105.7(7)	$\bar{1}$	0		0.83	0.52	this work
TOLDEG	2.928	0.112	105.7	$\bar{1}$	0		0.22	0	49
UGEHOG	2.928	0.112	109.0	$\bar{1}$	0		1.14	0.66	68
AQAQEQ	2.932	0.108	113.5	2_1	76		0	0.82	69
RUGHAE	2.937	0.103	105.7	$\bar{1}$	0		0.38	0	70
MERYAM	2.939	0.101	124.6	$2\perp$	65	166	0	0.43	71
VEQXIZ	2.948	0.092	108.6	$\bar{1}$	0		0	0.28	72
ZOLNIA	2.958	0.082	99.3	none	0		1.01	0	67
4'	2.9622(14)	0.078	104.2(13)	$\bar{1}$	0		0.42	0.26	this work
UYAVUN	2.966	0.074	88.2	none	2.6		0	0	73
NAZRIR	2.974	0.066	102.3	$\bar{1}$	0		1.06	0	74
MOBBOW	2.984	0.056	77.5	$2\perp$	60		0	0.74	75
ZIMDAD	3.000	0.040	112.1	$\bar{1}$	0		1.59	0.79	48
UPARUB	3.005	0.035	89.9	$\bar{1}$	0		0.62	0.77	76
FOMJIB	3.010	0.030	88.8	$\bar{1}$	0		0.11	0	77
2	3.0243(5)	0.016	107.9(13)	$\bar{1}$	0		0.04	0.69	this work
UGEHEW	3.027	0.013	108.0	none	7		0.99	0.74	68
NEYNOX	3.029	0.011	110.2	$\bar{1}$	0		1.15	0.78	78
Mean:	2.944		102	Min.:	0	166	0	0.17	
s.u.:	0.064		11	Max:	76	175	1.59	0.82	

[a] Refers to the radii of the two O atoms, irrespective of the H atom placement. [b] Disorder in the OH oxygen position may affect the accuracy of this short contact.

Table 7. Crystal Data and Structure Refinement Parameters [a]

Structure	**1**	**2**	**2a**	**2a'**	**2b**	**2c**
Formula	$C_{29}H_{39}OPSi$	$C_{26}H_{31}OP$	$C_{26}H_{31}OPS$	$C_{26}H_{31}OPS$	$C_{26}H_{31}OPSe$	$C_{26}H_{31}O_2P$
Solv. remov.	none	none	none	0.5 *m*-xyl.	none	none
FW	462.691	390.509	422.575	422.575	469.468	406.508
Temp./K	99.98(10)	99.99(10)	99.97(13)	100.01(10)	100.00(10)	99.99(10)
Cryst. Syst.	monoclinic	monoclinic	monoclinic	triclinic	monoclinic	monoclinic
Sp. Grp.	$P2_1/n$	$I2/a$	$P2_1/n$	$P\bar{1}$	$P2_1/n$	$P2_1/n$
a/Å	12.9736(1)	17.0476(2)	11.3753(1)	9.7793(2)	11.3228(1)	8.9681(1)
b/Å	14.1332(1)	13.4717(2)	13.4481(2)	11.6258(2)	13.4405(1)	12.7088(1)
c/Å	14.8182(1)	19.4796(2)	15.0529(2)	13.6112(2)	15.2927(2)	19.7044(2)
α/°	90	90	90	97.212(1)	90	90
β/°	96.655(1)	98.051(1)	97.205(1)	104.887(1)	97.743(1)	96.856(1)
γ/°	90	90	90	112.829(1)	90	90
Vol./Å^3	2698.74(3)	4429.59(10)	2284.55(5)	1333.60(4)	2306.09(4)	2229.73(4)
Z, Z'	4, 1	8, 1	4, 1	2, 1	4, 1	4,1
Data	5479	4503	4604	5363	4663	4530
Restr.	30	66	186	186	24	0
Param.	640	532	541	517	541	541
H treatment	aniso.	aniso.	aniso.	aniso.	aniso.	aniso.
R_1[b] [I ≥ 2σ(I)]	0.0137	0.0260	0.0172	0.0180	0.0207	0.0104
wR_2[c] [I ≥ 2σ(I)]	0.0323	0.0717	0.0443	0.0440	0.0539	0.0236
CCDC	2071681	2071684	2072749	2072750	2072751	2072752

[a] Refined with Olex2 using NoSpherA2 to generate anisotropic form factors from ED computed by DFT with ORCA 4.1 at the PBE/def2-TZVP level of theory; [b] $R_1 = \sum||F_o| - |F_c||/\sum|F_o|$; [c] $wR_2 = [\sum[w(F_o^2 - F_c^2)^2]/\sum w(F_o^4)]^{1/2}$.

Table 7. Crystal Data and Structure Refinement Parameters, cont.

Structure	**2c'**	**3**	**3a**	**3b**	**4**	**4a**
Formula	$C_{26}H_{31}O_2P$	$C_{52}H_{88}Cl_3O_3PSi_3$	$C_{51}H_{87}O_3PSi_3S$	$C_{51}H_{87}O_3PSeSi_3$	$C_{42}H_{63}O_3$	$C_{42}H_{63}O_3PS_{0.95}$
Solv. remov.	0.5 toluene	none	none	none	none	0.5 xylenes
FW	406.508	982.86	895.554	942.447	646.940	677.403
Temp./K	99.9(3)	100.01(10)	100.00(10)	99.99(10)	99.97(10)	100(1)
Cryst. Syst.	monoclinic	monoclinic	trigonal	trigonal	monoclinic	monoclinic
Sp. Grp.	$P2_1/c$	$P2_1/n$	$R3c$ [d]	$R3c$ [e]	$P2_1/c$	$P2_1/c$
a/Å	8.9534(3)	15.07865(16)	21.2320(2)	21.23208(17)	9.9347(1)	9.8864(1)
b/Å	12.7267(5)	29.2723(3)	21.2320(2)	21.23208(17)	20.8759(2)	21.1841(2)
c/Å	22.2246(8)	15.33640(15)	20.6906(2)	20.6661(2)	19.2929(2)	19.4175(2)
α/°	90	90	90	90	90	90
β/°	94.237(4)	114.0252(12)	90	90	103.699(1)	101.904(1)
γ/°	90	90	120	120	90	90
Vol./Å^3	2525.51(16)	6182.83(12)	8077.66(13)	8068.16(13)	3887.44(7)	3979.24(7)
Z, Z'	4, 1	4, 1	6, 0.33	6, 0.33	4, 1	4, 1
Data	6879	12468	3072	3233	7837	7944
Restr.	7	101	193	187	12	90
Param.	361	837	439	439	982	991
H treatment	iso. CH	iso. CH	iso. CH	iso. CH	aniso.	aniso.
R_1[b] [I ≥ 2σ(I)]	0.0597	0.0400	0.0131	0.0150	0.0176	0.0273
wR_2[c] [I ≥ 2σ(I)]	0.1515	0.0958	0.0368	0.0418	0.0403	0.0699
CCDC	2072753	2072754	2072755	2072756	2072757	2072758

[a] Refined with Olex2 using NoSpherA2 to generate anisotropic form factors from ED computed by DFT with ORCA 4.1 at the PBE/def2-TZVP level of theory; [b] $R_1 = \sum||F_o| - |F_c||/\sum|F_o|$; [c] $wR_2 = [\sum[w(F_o^2 - F_c^2)^2]/\sum w(F_o^4)]^{1/2}$; Flack: [d] -0.006(13), [e] 0.016(13).

Table 7. Crystal Data and Structure Refinement Parameters, cont.

Structure	**4a'**	**4b**	**4c**	**4c'**	**4c"**
Formula	$C_{42}H_{63}O_3PS$	$C_{42}H_{63}O_3PSe$	$C_{42}H_{65}O_5P$	$C_{42}H_{62.5}O_4P$	$C_{45}H_{69}O_{4.8}P$
Solv. removv.	none	0.5 xylenes	none	0.5 BuOH 0.5 H_2O	0.1 acetone
FW	679.006	725.85	680.955	662.446	717.82
Temp./K	99.98(10)	100.00(10)	99.99(10)	105(8)	100.01(10)
Cryst. Syst.	monoclinic	monoclinic	triclinic	tetragonal	triclinic
Sp. Grp.	$P2_1/c$	$P2_1/c$	$P\overline{1}$	$P4/n$	$P\overline{1}$
a/Å	9.7869(1)	9.8574(3)	10.2869(1)	28.2120(9)	15.9128(2)
b/Å	37.8693(4)	37.8826(12)	14.5269(3)	28.2120(9)	15.9128(2)
c/Å	11.6543(1)	11.6489(3)	14.6166(4)	12.8298(7)	19.4521(2)
α/°	90	90	78.344(2)	90	96.6880(10)
β/°	91.570(1)	91.484(2)	82.725(2)	90	104.3850(10)
γ/°	90	90	71.188(2)	90	107.7170(10)
Vol./Å^3	4317.73(7)	4348.5(2)	2020.48(8)	10211.5(9)	4466.31(10)
Z, *Z'*	4, 1	4, 1	2, 1	8, 1	4, 2
Data	8607	10638	8013	13929	18048
Restr.	494	44	30	378	76
Param.	665	656	722	991	1395
H treatment	iso. CH	iso. CH	iso. CH	aniso.	iso. CH
R_1[a] [I ≥ 2σ(I)]	0.0259	0.0339	0.0211	0.0393	0.0431
wR_2[a] [I ≥ 2σ(I)]	0.0677	0.0614	0.0569	0.0737	0.1016
CCDC	2072759	2072760	2072761	2072762	2072763

[a] Refined with Olex2 using NoSpherA2 to generate anisotropic form factors from ED computed by DFT with ORCA 4.1 at the PBE/def2-TZVP level of theory; [b] $R_1 = \sum||F_o| - |F_c||/\sum|F_o|$; [c] $wR_2 = [\sum[w(F_o^2 - F_c^2)^2]/\sum w(F_o^4)]^{1/2}$.

References

(1) Musina, E. I.; Balueva, A. S.; Karasik, A. A. Phosphines: preparation, reactivity and applications. In: *Organophosphorus Chemistry*, Allen, D. W., Loakes, D., Tebby, J. C., Eds.; Royal Society of Chemistry. **2019**, 48, 1-63.

(2) Musina, E. I.; Shamsieva, A. V.; Balueva, A. S.; Karasik, A. A. Tertiary phosphines: preparation and reactivity. In: *Organophosphorus Chemistry*, Allen, D. W., Loakes, D., Higham, L. J., Tebby, J. C. , Eds.; Royal Society of Chemistry. **2020**, 49, 1-63.

(3) Shiels, D.; Higham, L. J. Phosphines: preparation and reactivity. in *Organophosphorus Chem.* In: *Organophosphorus Chemistry*, Higham, L. J., Allen, D. W., Tebby, J. C. , Eds.; Royal Society of Chemistry. **2021**, 50, 1-36.

(4) Raj, J. G. J. Metal-organophosphine complexes: structure, bonding, and applications. *Rev. Inorg. Chem.* **2015**, 35, 25-56.

(5) James, S. L. Phosphines as building blocks in coordination-based self-assembly. *Chem. Soc. Rev*. **2009**, 38, 1744-1758.

(6) Schlatzer, T.; Breinbauer, R. Synthesis of Hydrophilic Phosphorus Ligands and Their Application in Aqueous-Phase Metal-Catalyzed Reactions. *Adv. Synth. Catal*. **2021**, 363, 668-687.

(7) Nishizawa, K.; Ouchi, M.; Sawamoto, M. Design of a hydrophilic ruthenium catalyst for metal-catalyzed living radical polymerization: highly active catalysis in water. *RSC Adv*. **2016**, 6, 6577-6582.

(8) Orton, G. R.; Pilgrim, B. S.; Champness, N. R. The chemistry of phosphines in constrained, well-defined microenvironments. *Chem. Soc. Rev.* **2021**, 50, 4411-4431.

(9) Biancalana, L.; Pratesi, A.; Chiellini, F.; Zacchini, S.; Funaioli, T.; Gabbiani, C.; Marchetti, F. Ruthenium arene complexes with triphenylphosphane ligands: cytotoxicity towards pancreatic cancer cells, interaction with model proteins, and effect of ethacrynic acid substitution. *New J. Chem.* **2017**, 41, 14574-14588.

(10) Biancalana, L.; Batchelor, L. K.; Palo, A. de; Zacchini, S.; Pampaloni, G.; Dyson, P. J.; Marchetti, F. A general strategy to add diversity to ruthenium arene complexes with bioactive organic compounds via a coordinated (4-hydroxyphenyl) diphenylphosphine ligand. *Dalton Trans.* **2017**, 46, 12001-12004.

(11) Biancalana, L.; Zacchini, S.; Ferri, N.; Lupo, M. G.; Pampaloni, G.; Marchetti, F. Tuning the cytotoxicity of ruthenium (II) *para*-cymene complexes by mono-substitution at a triphenylphosphine/phenoxydiphenylphosphine ligand. *Dalton Trans.* **2017**, 46, 16589-16604.

(12) Biancalana, L.; Ciancaleoni, G.; Zacchini, S.; Monti, A.; Marchetti, F.; Pampaloni, G. Solvent-dependent hemilability of (2-diphenylphosphino) phenol in a Ru (II) para-cymene system. *Organometallics*. **2018**, 37, 1381-1391.

(13) Honorato, J.; Oliveira, K. M.; Leite, C. M.; Colina-Vegas, L.; Nóbrega, J. A.; Castellano, E. E.; Ellena, J.; Correa, R. S.; Batista, A. A. "Half-Sandwich"/RuII Anticancer Complexes Containing Triphenylphosphine and *p*-Substituted Benzoic Acids. *J. Braz. Chem. Soc.* **2020**, 31, 2237-2249.

(14) Guimarães, I. D. L.; Garcia, J. R.; Wohnrath, K.; Boeré, R. T. Chemical and Electrochemical Oxidation of *Tris*(3,5-di-tert-butylphenyl) phosphine–High Z' Crystal Structures and Conformational Effects Associated with Bulky meta Substituents. *Eur. J. Inorg. Chem*. **2018**, 2018, 3606-3614.

(15) Guimarães, I. D. L.; Marszaukowski, F.; Ribeiro, R.; de Lazaro, S. R.; de Oliveira, K. M.; Batista, A. A.; Castellen, P.; Wrobel, E.; Garcia, J. R.; Boeré, R. T.; Wohnrath, K. Synthesis and characterization of η^6-*p*-cymene ruthenium (II) complexes containing alkyl-and methoxy-substituted triarylphosphines. *J. Organomet. Chem.* **2021**, 931, 121599.

(16) Pastor, S. D.; Hessell. E. T. Organophosphorus and organosilicon derivatives of sterically hindered phenols. *J. Organomet. Chem.* **1989**, 376, 21-29.

(17) Muller, E.; Eggensperger, H.; Scheffier, K. Electron paramagnetic resonance absorption measurements of organic compounds containing paramagnetic phosphorus. *Justus Liebigs Ann. Chem.* **1962**, 658, 103-12.

(18) Kleemiss, F.; Dolomanov, O.V.; Bodensteiner, M.; Peyerimhoff, N.; Midgley, M.; Bourhis, L.J.; Genoni, A.; Malaspina, L.A.; Jayatilaka, D.; Spencer, J.L.; White, F.; Grundkoetter-Stock, B.; Steinhauer, S.; Lentz, D.; Puschmann, H.; Grabowsky, S. Accurate crystal structures and chemical properties from NoSpherA2. *Chem. Sci.* **2021**, 12, 1675-1692.

(19) Dolomanov, O. V.; Bourhis, L. J.; Gildea, R. J; Howard, J. A. K.; Puschmann, H. J. OLEX2: a complete structure solution, refinement and analysis program. *Appl. Cryst.* **2009**, 42, 339-341.

(20) Jeffrey, G. A. *An introduction to hydrogen bonding*; Oxford university press: New York, 1997, Vol.12, pp 330.

(21) Grabowski, S. J. Chapter 1: Hydrogen Bond – Definitions, Criteria of Existence and Various Types. In: *Understanding Hydrogen Bonds: Theoretical and Experimental Views*, Grabowski, S. J., Ed.; Royal Society of Chemistry, 2021, pp. 1-40.

(22) Steiner, T. The hydrogen bond in the solid state. *Angew. Chem. Int. Ed.* **2002**, 41, 48-76.

(23) Lutz, M.; Spek, A. L. 2,6-Di-tert-butylphenol revisited at 110 K. *Acta Crystallogr., C Cryst. Struct. Commun.* **2005**, 61, o639-o641.

(24) Vilčiauskas, L.; Tuckerman, M. E.; Bester, G.; Paddison, S. J.; Kreuer, K. D. The mechanism of proton conduction in phosphoric acid. *Nat. Chem*. **2012**, 4, 461-466.

(25) Blackholly, L. R.; Shepherd, H. J.; Hiscock, J. R. 'Frustrated' hydrogen bond mediated amphiphile self-assembly–a solid state study. *Cryst. Eng. Comm*. **2016**, 18, 7021-7028.

(26) Hiscock, J. R.; Bustone, G. P.; Wilson, B.; Belsey, K. E.; Blackholly, L. R. In situ modification of nanostructure configuration through the manipulation of hydrogen bonded amphiphile self-association. *Soft Matter*. **2016**, 12, 4221-4228.

(27) Zhan, T. G.; Zhou, T. Y.; Qi, Q. Y.; Wu, J.; Li, G. Y.; Zhao, X. The construction of supramolecular polymers through anion bridging: from frustrated hydrogen-bonding networks to well-ordered linear arrays. *Polym. Chem.* **2015**, 6, 7586-7593.

(28) Io, A.; Kawatsu, T.; Tachikawa, M. Quantum stabilization of the frustrated hydrogen bonding structure in the hydrogen fluoride trimer. *J. Phys. Chem. A*. **2019**, 123, 7950-7955.

(29) Gumbs, T. L.; White, L. J.; Wells, N. J.; Shepherd, H. J.; Hiscock, J. R. 'Frustrated' hydrogen-bonded self-associated systems as templates towards DNA incorporated nanostructure formation. *Supramol. Chem*. **2018**, 30, 286-295.

(30) Marszaukowski, F.; Wohnrath, K.; Boeré, R. T. Bulky 2, 6-disubstituted aryl siloxanes and a disilanamine. *Acta Crystallogr. E*. **2020**, 76, 318-323.

(31) Denniston, M. L.; Martin, D. R. Methyldiphenylphosphine Oxide and Dimethylphenylphosphine Oxide. *Inorg. Synth.* **1977**, 17, 183–185.

(32) Capps, K. B.; Wixmerten, B.; Bauer, A.; Hoff, C. D. Thermochemistry of Sulfur Atom Transfer. Enthalpies of Reaction of Phosphines with Sulfur, Selenium, and Tellurium, and of Desulfurization of Triphenylarsenic Sulfide, Triphenylantimony Sulfide, and Benzyl Trisulfide. *Inorg. Chem*. **1998**, 37, 2861–2864.

(33) Kühl, O. *Phosphorus-31 NMR spectroscopy: a concise introduction for the synthetic organic and organometallic chemist*; Springer-Verlag: Berlin Heidelberg, 2008, pp.132.

(34) Cinderella, A. P.; Vulovic, B.; Watson, D. A. Palladium-catalyzed cross-coupling of silyl electrophiles with alkylzinc halides: a Silyl-Negishi reaction. *J. Am. Chem. Soc.*, **2017**, 139, 7741-7744.

(35) Boeré, R. T.; Bond, A. M.; Cronin, S.; Duffy, N. W.; Hazendonk, P.; Masuda, J. D.; Zhang, Y. Photophysical, dynamic and redox behavior of *tris*-(2,6-diisopropylphenyl) phosphine. *New J. Chem.* **2008**, 32, 214-231.

(36) Muller, A.; Otto, S.; Roodt, A. Rapid phosphorus (III) ligand evaluation utilising potassium selenocyanate. *Dalton Trans.* **2008**, 650-657.

(37) Beckmann, U.; Süslüyan, D.; Kunz, P. C. Is the $^{1}J_{PSe}$ Coupling Constant a Reliable Probe for the Basicity of Phosphines? A ^{31}P NMR Study. *Phosphorus Sulfur Silicon Relat. Elem.* **2011**, 186, 2061-2070.

(38) Palidwar, S. M.; Boeré, R.T., unpublished results.

(39) Muller, A. Bis(2,4-dimethoxyphenyl)(phenyl) phosphine selenide. *Acta Crystallogr., Sect. E.* **2011**, 67, o97-o97.

(40) Allen, D. W.; Nowell, I. W.; Taylor, B. F. The chemistry of heteroaryl phosphorus compounds. Part 16. Unusual substituent effects on selenium-77 nuclear magnetic resonance chemical shifts of heteroaryl-and aryl-phosphine selenides. X-Ray crystal structure of tri(2-furyl)phosphine selenide. *J. Chem. Soc., Dalton Trans.* **1985**, 2505-2508.

(41) Gáti, T.; Simon, A.; Tóth, G.; Magiera, D.; Moeller, S.; Duddeck, H. Adducts of $Rh_2[MTPA]_4$ with some phosphine chalcogenides: nature of binding and ligand exchange. *Magn. Reson. Chem.* **2004**, 42, 600-604.

(42) Muller, A.; Meijboom, R. Tris(4-fluorophenyl)phosphine selenide. *Acta Crystallogr., Sect. E.* **2007**, 63, o4055-o4055.

(43) Samb, I.; Bell, J.; Toullec, P. Y.; Michelet, V.; Leray, I. Fluorescent phosphane selenide as efficient mercury chemodosimeter. *Org. Lett.* **2011**, 13, 1182-1185.

(44) Howell, J. S.; Fey, N.; Lovatt, J. D.; Yates, P. C.; McArdle, P.; Cunningham, D.; Sadeh, E.; Gottlieb, H. E.; Golschmidt, Z.; Hursthouse, M. B.; Light, M. E. Effect of fluorine and trifluoromethyl substitution on the donor properties and stereodynamical behaviour of triarylphosphines. *J. Chem. Soc., Dalton Trans.* **1999**, 3015-3028.

(45) Poverenov, E.; Shimon, L. J.; Milstein, D. Quinone methide generation based on a *cis*-(N,N) platinum complex. *Organometallics*. **2007**, 26, 2178-2182.

(46) Satoh, Y.; Shi, C. An Efficient Synthesis of 4-Aryl-2,6-di-*tert*-butylphenols by a Palladium-Catalyzed Cross-Coupling Reaction. *Synthesis*. **1994**, 1994, 1146-1148.

(47) Kumar, H.; Patel, M.; Mohan, D. Simplified batch and fixed-bed design system for efficient and sustainable fluoride removal from water using slow pyrolyzed okra stem and black gram straw biochars. *ACS Omega*. **2019**, 4, 19513-19525.

(48) Sharma, B. M.; Rathod, J.; Gonnade, R. G.; Kumar, P. Harnessing Nucleophilicity of Allenol Ester with *p*-Quinone Methides via Gold Catalysis: Application to the Synthesis of Diarylmethine-Substituted Enones. *J. Org. Chem.* **2018**, 83, 9353-9363.

(49) Liu, Z. Q.; Tang, M.; Zhang, L. D.; You, P. S.; Liu, S. S. The crystal structure of 2,6-di-*tert*-butyl-4-(phenyl(phenylsulfonyl)methyl) phenol, $C_{27}H_{32}O_3S$. *Z. Krist-New Cryst. St.* **2019**, 234, 703-705.

(50) Mislow, K. Stereochemical consequences of correlated rotation in molecular propellers. *Acc. Chem. Res.* **1976**, 9, 26-33.

(51) Groom, C. R.; Bruno, I. J.; Lightfoot, M. P.; Ward, S. C. The Cambridge Structural Database. *Acta Cryst. B*, **2016**, 72, 171‑179.

(52) Allen, F. H.; Bruno, I. J. Bond lengths in organic and metal-organic compounds revisited: X—H bond lengths from neutron diffraction data. *Acta Cryst. B.* **2010**, 66, 380-386.

(53) Zheng, L.; Zheng, D.; Wang, Y.; Yu, C.; Zhang, K.; Jiang, H. Chiral bisphosphine ligands based on quinoline oligoamide foldamers: application in asymmetric hydrogenation. *Org. Biomol. Chem.* **2019**, 17, 9573-9577.

(54) Gowrisankar, S.; Sergeev, A. G.; Anbarasan, P.; Spannenberg, A.; Neumann, H.; Beller, M. A General and Efficient Catalyst for Palladium-Catalyzed C−O Coupling Reactions of Aryl Halides with Primary Alcohols. *J. Am. Chem. Soc.* **2010**, 132, 11592-11598.

(55) Bigler, R.; Otth, E.; Mezzetti, A. Chiral Macrocyclic N_2P_2 Ligands and Iron(II): A Marriage of Interest. *Organometallics*. **2014**, 33, 4086-4099.

(56) Wang, J.; Liu, C.; Liu, X.; Shao, L.; Zhang, X. M. C—H··· O hydrogen bonding interactions for sterically hindered phenols and their phenoxyl radicals. *J. Phys. Org. Chem.* **2019**, 32, e3927.

(57) Hill, N. D. D.; Boeré, R. T. Two *tris*(3,5-disubstituted phenyl) phosphines and their isostructural P^V oxides. *Acta Crystallogr. E*. **2018**, 74, 889-894.

(58) Finnen, D. C.; Pinkerton, A. A. The Structures of the Bulky Basic Phosphine Sulfides *Tris*(2,6-Dimethoxyphenyl)Phosphine Sulfide (DMPP=S) and *Tris*(2,4,6-Trimethoxyphenyl) Phosphine Sulfide (TMPP[dbnd]S). *Phosphorus Sulfur Silicon Relat. Elem.* **1994**, 90, 11-19.

(59) Raymundo, M.; Padgett, C. W.; Lynch, W. E. *Tris*(4-methoxyphenyl) phosphine selenide. *IUCrData*. **2016**, 1, x161271.

(60) Allen, D. W.; Bell, N. A.; March, L. A.; Nowell, I. W. Crystallographically determined Se=O and P=O interactions in *tris*(2,4-dimethoxyphenyl) phosphine selenide and the 2,4,6-trimethoxy analogue. Correlations of P=Se bond lengths with ^{77}Se NMR data. *Polyhedron*. **1990**, 9, 681-685.

(61) Bernstein, J. Peggy Etter: A Personal Recollection. *Cryst. Growth Des.* **2016**, *16*, 1135–1143

(62) Etter, M. C. Encoding and decoding hydrogen-bond patterns of organic compounds. *Acc. Chem. Res.* **1990**, 23, 120-126.

(63) Yan, J.; Chen, M.; Sung, H. H. Y.; Williams, I. D.; Sun, J. An organocatalytic asymmetric synthesis of chiral β, β-diaryl-α-amino acids via addition of azlactones to in situ generated para-quinone methides. *Chem. Asian J.* **2018**, 13, 2440-2444.

(64) Balashova, T. V.; Rumyantsev, R. V.; Fukin, G. K.; Pushkarev, A. P.; Maleev, A. A.; Shpakovskii, D. B.; Antonenko, T. A.; Milaeva, E. R.; Bochkarev, M. N. Lanthanide complexes with the Schiff base containing sterically hindered phenol: Synthesis, structure, and luminescence properties. *Russ. J. Coord. Chem.* **2017**, 43, 852-857.

(65) Nishide, H.; Maeda, T.; Oyaizu, K.; Tsuchida, E. High-spin polyphenoxyl based on poly (1, 4-phenyleneethynylene). *J. Org. Chem.* **1999**, 64, 7129-7134.

(66) Yehye, W. A.; Abdul Rahman, N. A.; Alhadi, A.; Khaledi, H.; Ng, S. W.; Ariffin, A. Butylated hydroxytoluene analogs: Synthesis and evaluation of their multipotent antioxidant activities. *Molecules*. **2012**, 17, 7645-7665.

(67) Dorofeeva, V. N.; Pavlishchuk, A. V.; Kiskin, M. A.; Efimov, N. N.; Minin, V. V.; Lytvynenko, A. S.; Gavrilenko, K. S.; Kolotilov, S. V.; Novotortsev, V. M.; Eremenko, I. L. CoII Complexes with a tripyridine ligand, containing a 2,6-di-*tert*-butylphenolic fragment: synthesis, structure, and formation of stable radicals. *ACS omega*. **2019**, 4, 203-213.

(68) Payne, D. T.; Webre, W. A.; Gobeze, H. B.; Seetharaman, S.; Matsushita, Y.; Karr, P. A.; Chahal, M. K.; Labuta, J.; Jevasuwan, W.; Fukata, N.; Fossey, J. S.; Ariga, K.; D'Souza, F.; Hill, J. P. Nanomolecular singlet oxygen photosensitizers based on hemiquinonoid-resorcinarenes, the fuchsonarenes. *Chem. Sci.* **2020**, 11, 2614-2620.

(69) Jarava-Barrera, C.; Parra, A.; López, A.; Cruz-Acosta, F.; Collado-Sanz, D.; Cárdenas, D. J.; Tortosa, M. Copper-catalyzed borylative aromatization of p-quinone methides: enantioselective synthesis of dibenzylic boronates. *ACS Catal.* **2016**, 6, 442-446.

(70) Porter, T. R.; Kaminsky, W.; Mayer, J. M. Preparation, structural characterization, and thermochemistry of an isolable 4-arylphenoxyl radical. *J. Org. Chem.* **2014**, 79, 9451-9454.

(71) Gao, Y. Y.; Hua, Y. Z.; Wang, M. C. Asymmetric 1, 6-Conjugate Addition of para-Quinone Methides for the Synthesis of Chiral β, β-Diaryl-α-Hydroxy Ketones. *Adv. Synth. Catal.* **2018**, 360, 80-85.

(72) Hill, J. P.; Wakayama, Y.; Schmitt, W.; Tsuruoka, T.; Nakanishi, T.; Zandler, M. L.; McCarty, A. L.; D'Souza, F.; Milgrom, L. R.; Ariga, K. Regulating the stability of 2D crystal structures using an oxidation state-dependent molecular conformation. *Chem. Commun.* **2006**, 2320-2322.

(73) Rathi, P.; Chahal, M. K.; Sankar, M. *CSD Communication*. **2016**

(74) Ding, W.; Liu, Z.; Tian, L.; Quan, X. Synthesis, characterization, and in vitro cytotoxicity of triorganotin 3, 5-di-*tert*-butyl-4-hydroxybenzoates. *Synth. React. Inorg., Met.-Org., Nano-Met .Chem*. **2012**, 42, 82-87.

(75) Takahashi, M.; Ogino, H.; Kobayashi, K. Multimelting Behavior and Glass Transition of Monotropic Polymorphs of 3, 5-Diphenyl-4-hydroxyphenyl-substituted Galvinol. *Chem. Lett.* **2014**, 43, 187-189.

(76) Zhou, S.; Cai, B.; Hu, C.; Cheng, X.; Li, L.; Xuan, J. Visible light and base promoted OH insertion/cyclization of para-quinone methides with aryl diazoacetates: An approach to 2, 3-dihydrobenzofuran derivatives. *Chin. Chem. Lett.* **2021**, 32, 2577-2581.

(77) Rezende, M. C.; Dominguez, M.; Wardell, J. L.; Skakle, J. M.; Low, J. N.; Glidewell, C. Supramolecular structures of five 5-(arylmethylene)-1,3-dimethylpyrimidine-2,4,6(1H,3H,5H)-triones: isolated molecules, hydrogen-bonded chains and chains of fused hydrogen-bonded rings. *Acta Crystallogr. C*. **2005**, 61, o306-o311.

(78) Sharma, B. M.; Shinde, D. R.; Jain, R.; Begari, E.; Satbhaiya, S.; Gonnade, R. G.; Kumar, P. Unravelling the Nucleophilicity of Butenolides for 1,6-Conjugate Addition to *p*-Quinone Methides: A Direct Access to Diversely Substituted Butenolide-Derived Diarylmethanes. *Org. Lett.* **2018**, 20(9), 2787-2791.

(79) Chen, T. R.; Lee, H. P.; Chen, J. D. Water Attack Umpolung Aromatic Systems to Release Hydrogen. *Inorg. Chem.* **2011**, 50, 3645-3650.

(80) Siefert, R.; Weyhermüller, T.; Chaudhuri, P. Isolation, structural and spectroscopic investigations of complexes with tridentate [O,P,O] and [O,O,O] donor ligands. *J. Chem. Soc., Dalton Trans.* **2000**, 4656-4663.

(81) Ribeiro da Silva, M. A. V.; Matos, M. A. R.; Morais, V. M. F.; Miranda, M. S. Thermochemical and Theoretical Study of *tert*-Butyl and Di-*tert*-butylphenol Isomers. *J. Org. Chem.* **1999**, 64, 8816-8820.

(82) Bewick, N. A.; Arendt, A.; Li, Y.; Szafert, S.; Lis, T.; Wheeler, K. A.; Young, J.; Dembinski, R. Synthesis and Solid-State Structure of (4-Hydroxy-3,5-diiodophenyl) phosphine Oxides. Dimeric Motifs with the Assistance of OH··· O= P Hydrogen Bonds. *Curr. Org. Chem*. **2015**, 19, 469-474.

(83) Perrin, D. D.; Armarego, W. L. F. *Purification of laboratory chemicals;* Butterworth-Heinemann: Oxford, 1996, 4th ed., pp. 529.

(84) Lucente-Schultz, R. M.; Moore, V. C.; Leonard, A. D.; Price, B. K.; Kosynkin, D. V.; Lu, M.; Partha, R.; Conyers, J. L; Tour, J. M. Antioxidant single-walled carbon nanotubes. *J. Am. Chem. Soc.* **2009**, 131, 3934-3941.

(85) *CrysAlis PRO* v.1.171.41.67a (Rigaku Oxford Diffraction, 2020).

(86) Sheldrick, G. M. SHELXT - Integrated space-group and crystal-structure determination. *Acta Cryst.* **2015**, A71, 3-8.

(87) Sheldrick, G. M. Crystal structure refinement with SHELXL. *Acta Crystallogr., Sect. C: Struct. Chem.* **2015**, C71, 3-8.

(88) Neese, F. Software update: the ORCA program system, version 4.0. *WIREs Comp. Mol. Sci.* **2018**, 8, e1327.

(89) Macrae, C. F.; Sovago, I.; Cottrell, S. J.; Galek, P. T. A.; McCabe, P.; Pidcock, E.; Platings, M.; Shields, G. P.; Stevens, J. S.; Towler, M.; Wood, P. A. Mercury 4.0: from visualization to analysis, design and prediction *J. Appl. Cryst.* **2020**, 53, 226-235.

(90) Frisch, M. J.; Trucks, G. W.; Schlegel, H. B.; Scuseria, G. E.; Robb, M. A.; Cheeseman, J. R.; Scalmani, G.; Barone, V.; Petersson, G. A.; Nakatsuji, H.; Li, X.; Caricato, M.; Marenich, A. V.; Bloino, J.; Janesko, B. G.; Gomperts, R.; Mennucci, B.; Hratchian, H. P.; Ortiz, J. V.; Izmaylov, A. F.; Sonnenberg, J. L.; Williams-Young, D.; Ding, F.; Lipparini, F.; Egidi, F.; Goings, J.; Peng, B.; Petrone, A.; Henderson, T.; Ranasinghe, D.; Zakrzewski, V. G.; Gao, J.; Rega, N.; Zheng, G.; Liang, W.; Hada, M.; Ehara, M.; Toyota, K.; Fukuda, R.; Hasegawa, J.; Ishida, M.; Nakajima, T.; Honda, Y.; Kitao, O.; Nakai, H.; Vreven, T.; Throssell, K.; Montgomery, J. A., Jr.; Peralta, J. E.; Ogliaro, F.; Bearpark, M. J.; Heyd, J. J.; Brothers, E. N.; Kudin, K. N.; Staroverov, V. N.; Keith, T. A.; Kobayashi, R.; Normand, J.; Raghavachari, K.; Rendell, A. P.; Burant, J. C.; Iyengar, S. S.; Tomasi, J.; Cossi, M.; Millam, J. M.; Klene, M.; Adamo, C.; Cammi, R.; Ochterski, J. W.; Martin, R. L.; Morokuma, K.; Farkas, O.; Foresman, J. B.; Fox, D. J. Gaussian 16, revision B.01; Gaussian, Inc.: Wallingford, CT, 2016.

(91) Dennington, R.; Keith, T. A.; Millam, J. M. GaussView, version 6.0; Semichem, Inc.: Shawnee Mission, KS, 2016.

(92) Goerigkab, L.; Grimme, S. A thorough benchmark of density functional methods for general main group thermochemistry, kinetics, and noncovalent interactions. *Phys. Chem. Chem. Phys*. **2011**, 13, 6670−6688.

(93) Grimme, S.; Hansen, A.; Brandenburg, J. G.; Bannwarth, C. Dispersion-corrected mean-field electronic structure methods. *Chem. Rev.* **2016**, 116, 5105–5154.

For Table of Contents Use Only

Frustrated and Realized Hydrogen Bonding in 4-Hydroxy-3,5-di*tert*butylphenylphosphine Derivatives

Flávia Marszaukowski, René T. Boeré* and Karen Wohnrath*

TOC Graphic and Text – this is prepared to the 'actual size' for printing, 6 x 3.5 cm.

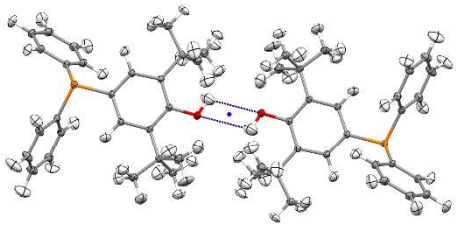

Steric congestion from the flanking *tert*butyl groups 'frustrates' conventional hydrogen bonding, resulting in the weak double contact. But with stronger acceptors, H-bonding is enabled.